NMR Probeheads for *In Vivo* Applications

AXEL HAASE, FLORIAN ODOJ, MARKUS VON KIENLIN, JAN WARNKING, FLORIAN FIDLER, ALEXANDER WEISSER, MATHIAS NITTKA, EBERHARD ROMMEL, TITUS LANZ, BERNHARD KALUSCHE, MARK GRISWOLD

Physikalisches Institut, Universität Würzburg, Würzburg, Germany

ABSTRACT: The NMR probehead is a key element of the receiving chain of an NMR spectrometer. To optimize the signal-to-noise ratio the probehead must be adapted for the specific application. This article describes the basic physics and characteristics of NMR probeheads for *in vivo* applications in small animals and plants as well as quality control procedures on the workbench and in the NMR spectrometer. Various probeheads including volume coils, surface coils, double tuned coils, and microscopy coils are presented and illustrated by results of specific *in vivo* applications. © 2000 John Wiley & Sons, Inc. Concepts Magn Reson 12: 361–388, 2000

KEY WORDS: radio frequency; magnetic resonance; imaging; spectroscopy; dual tuned coils; volume coils; surface coils; microscopy coils

INTRODUCTION

NMR imaging and spectroscopy have become a powerful diagnostic procedure in modern medicine to noninvasively analyze the anatomy, function, and biochemistry of the human body. NMR also offers scientists in a broad area of biomedical research an important method for animal and organ studies. Additionally, *in vivo* biochemical investigations of animals for pharmaceutical research and development use NMR as an additional tool to complement other laboratory analytical tools.

Most NMR investigations in medicine and biology require a high spatial, spectral, and time resolution and thus a large signal-to-noise ratio (SNR). Several improvements of the NMR spectrometer design have allowed this to be obtained on standard equipment. Today it is possible to acquire NMR spectra from nanoliter volumes and tenths of millimole metabolite concentrations. The recent introduction of high magnetic fields of up to 8 T in human studies and 17.6 T in animal research offers one additional avenue to expand the achievable SNR. This has been used in many cases to improve the achievable spatial resolution, resulting in resolutions under 1 mm in human examinations, while the resolution in NMR microscopy (*1*) has even approached 10 μm.

An important step forward in the optimization of the SNR is the design of NMR probeheads. During the last 25 years, many interesting new ideas for NMR coils have been described. A local 'surface coil', a concept from the early days of NMR (*2*), was the first innovation which made *in vivo* NMR spectroscopy possible (*3*). With the advent of high magnetic fields for human applica-

Received 28 December 1999; revised 13 May 2000; accepted 15 May 2000.

Correspondence to: Prof. Dr. Axel Haase; E-mail: haase@physik.uni-wuerzburg.de

Concepts in Magnetic Resonance, Vol. 12(6) 361–388 (2000)

tions, new designs of NMR resonators were necessary. During the last ten years, multiple receiving coils, or 'phased array coils' have further improved the signal-to-noise ratio that can be achieved in an NMR experiment (*4*). Finally, since multinuclear NMR experiments are possible in high field systems, many versions of double- or triple-tuned coils have been described (*5*).

This article will introduce the basic physics and characteristics of NMR probeheads. All important design concepts for volume coils, surface coils, and double tuned coils will be discussed and applications shown. Important steps in the optimization of coils, preamplifier design, and quality control will also be presented. Using this article, readers should be able to understand the different coil techniques and their relative advantages, and to start to design their own NMR probeheads for *in vivo* studies. To make comprehension of this article easier for the novice, a glossary at the end of this contribution contains a short list of useful physical quantities and technical descriptions used throughout. The first use in each chapter of those items contained in the glossary are shown in bold typeface.

PRINCIPLES OF SENSITIVITY

The NMR Probehead

The NMR probehead is the key element of the receiving chain of an NMR spectrometer. It consists of the radiofrequency (RF) coil in which the signal is detected, the coupling network, and the mechanical holding device. The coil can be used both for transmission of RF power to the sample and detection of the NMR signal. It is also possible to split these functions to two separate coils, with one dedicated for transmission and the other for reception. An optimized probehead has to meet several requirements. One of the most stringent demands is that the coil has to have optimal sensitivity in the region of interest (ROI). In addition, there are many other substantial requirements, whose relative importance depends on each specific application. The homogeneity of the magnetic field produced by the coil, given by the B_1 field, has to meet the requirements of the experiment. Furthermore, the materials used in the construction of the probehead must not reduce the homogeneity of the static magnetic field B_0. Seldom mentioned, but nevertheless important for the routine usage of the probehead, is mechanical stability which must match the demands of the application. The installation of the probehead into the spectrometer should be kept simple so that a precise and reproducible positioning should be as easy as possible. Comfortable access to the sample and the rods used for tuning and matching of the coil should be secured. In addition, *in vivo* probeheads often require the facility of sample temperature control, electrocardiogram (ECG) monitoring, anaesthesia, and oxygen delivery, etc.

The requirements described above represent only an overview of what has to be considered for the design and construction of a probehead. Every application has its own demands, so the ideal probehead should be designed to meet these individual requirements—there is no single optimal coil for every application!

The Signal-to-Noise Ratio

The parameter that we are most interested in when describing the coil performance is the ratio of the induced signal voltage to the received noise voltage, or the signal-to-noise ratio (SNR). In order to describe the mechanisms of signal and noise generation, a simple model of the NMR coil is sufficient. The properties of the NMR coil can be summarized in an equivalent circuit (Fig. 1). In this circuit, the inductance L of the receiving coil is in series with the resistance R in which all loss mechanisms are combined. V is the induced NMR signal voltage, which is superimposed by the noise voltage N. The origin of both the signal and noise voltages is the topic of the following two sections.

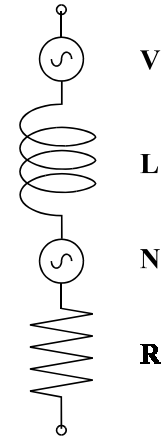

Figure 1 Equivalent circuit of an NMR coil. Signal strength V is induced in the inductance L. Noise voltage N is generated by the resistance R.

The NMR Signal

If a current is passed through the inductor L, a magnetic field B_1 will be created. The B_1 field of this coil will decrease with increasing distance from the inductor. For example, consider two spins located at different points A and B (Fig. 2). The B_1 field strength generated at point A will in general be larger than at point B, since it is closer to the coil. But what we are really interested in is the signal induced by the two spins in the coil during reception. It can easily be shown that the signal induced by spin A during reception will be larger than the signal induced by spin B. The principle of reciprocity (*6*) establishes this correspondence between the transmission and the reception characteristics of an NMR coil. The important conclusion of this principle is that the B_1 field strength of a coil at any point in space at a fixed power during transmission is equivalent to the sensitivity during detection. Therefore, to maximize the received signal, we would like to maximize the B_1 field in the sample. There are two essential properties of the coil needed to achieve this. First, the coil dimensions should match the sample dimensions as closely as possible. This is described quantitatively by the concept of the filling factor (*7*, *8*). In general, a high filling factor is desirable for NMR coils. Second, all loss mechanisms should be reduced to achieve a high sensitivity. This is quantified in general by the **quality factor**, which will be discussed below. These two quantities taken together give an indication of the absolute sensitivity (*9*).

The Noise

In the equivalent circuit (Fig. 1), the resistance R is the sum of all the resistances r_i that can be attributed to the different loss mechanisms found in NMR coils given by

$$R = \sum r_i \qquad [1]$$

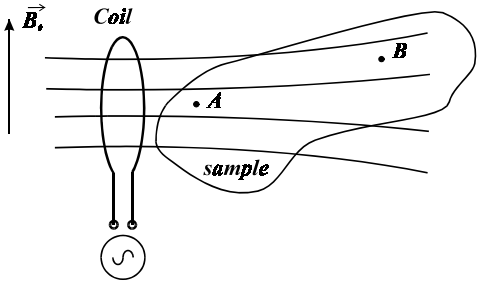

Figure 2 Principle of reciprocity.

In NMR applications, the noise voltage N can be calculated as thermal noise of this resistance (*10*) given by

$$N = \sqrt{4kTR\Delta\nu} \qquad [2]$$

N depends on the acquisition bandwidth $\Delta\nu$, the magnitude of R and the temperature T of the noise resistance, and k, Boltzmann's constant. Equation [2] establishes another equivalence of transmission and reception, since any loss mechanism (R) occurring during transmission represents a noise mechanism (N) during reception. However, in contrast to the principle of reciprocity, the noise during reception is weighted by the temperature T of the resistance. This temperature does not affect the losses during transmission (except for the temperature dependency of r_i).

In most NMR applications (with the exception of cooled copper coils and superconducting coils), the only term in Eq. [2] which can be controlled in the design of the probehead is the total resistance in the equivalent circuit of the coil. In the following, we discuss the four main contributions to this resistance and how they relate to the design of an optimal probehead.

Losses Within the Wires. These losses are caused by the ohmic resistance of the wire and depend on the specific conductivity and the geometry of the wire employed. This resistance is typically decreased as the cross section of the wire is increased, while the resistance increases with increasing length of wire. However, at higher frequencies, such as those used in NMR, the resistance of the wire is much greater than the resistance at low frequencies because of the **skin effect**. This effect describes the fact that current flows only on the outer surface of the wire at higher frequencies. Coupling between different parts of a coil results in an additional force on the electrons and is described as proximity effect. This effect can result in a further increase in the resistance when wires are placed close together, for example in tightly wound solenoidal coils (*6*). In addition to the ohmic losses in the wire, other components used in the transfer of the signal to the receiver of the NMR system, such as the coupling network and cable, can be lossy.

All of these losses can be minimized through the use of low loss components and by optimizing the geometry, placement, and conductivity of the

wires and other components of the coil. Numerical optimizations can be particularly helpful in this regard. However, the losses in the wires and other components are typically only a concern for the design of microscopy or low field probeheads, where this loss mechanism dominates the total losses.

Losses due to Magnetic Interactions in the Near Field of the Coil. During transmission, the NMR coil produces the fluctuating magnetic field B_1 in the **near field** of the coil. According to Maxwell's Laws, this fluctuating B_1 field will induce RF currents in any conducting material within the field, including the sample. Since conducting materials are typically lossy, some of the transmitted power is dissipated. Applying the principle of reciprocity, these RF currents represent a noise mechanism during signal reception.

Since the magnetic coupling between sample and coil is mandatory for reception of the NMR signal, the losses in the sample originating from this mechanism cannot be avoided, but can be minimized with proper coil design. The easiest way to optimize this is to ensure that the magnetic field interacts only with the ROI of the sample. In addition, the axial component of the B_1 field should be minimized, since it does not contribute any signal, although it can contribute noise. Normally, losses due to this mechanism are important in *in vivo* samples, especially at high fields, or in other large conductive samples (*11*).

Losses due to Electric Interactions in the Near Field of the Coil. Electric fields in the near field of the coil are caused by potential differences between different parts of the coil. These electric fields generate dissipative RF currents in all conductive materials within the field, such as the sample. In dielectric media these fields generate displacement currents. If the dielectric has associated losses, these currents contribute to the noise without any contribution to the signal. Materials are described with respect to their dielectric losses by the **loss angle tan δ**.

The main sources of electric fields in an NMR coil are capacitors. The losses caused by their stray fields can be avoided by screening the local electric field with conductive materials. In addition, all parts of the probehead in the near field of the coil should be selected with respect to their dielectric losses. Once these contributions are minimized, the remaining losses due to electric fields located in the sample can be diminished by designing the coil dimensions to match the dimensions of the ROI as closely as possible. As with magnetic interactions, the losses due to these electrical interactions are important in *in vivo* samples at high fields, or in other large conductive samples.

Losses due to the Electromagnetic Radiation. The fields generated by the NMR coil can be divided into two different parts: the near field and the **far field**. Since only the near field is used for NMR detection, radiation of energy into the far field represents another loss mechanism. However, this process can easily be avoided by using radiation shields. RF shielding performs another important task in the suppression of interfering external signals, which is, for example, the aim of Faraday cages for whole body scanners. In addition to RF shielding, one must ensure that radiative losses are minimized by avoiding the use of wire lengths which are in the range of a wavelength. Since these methods are easy to implement, radiative losses usually only play a minor role in the overall noise of NMR experiments, except for large coils at very high field strengths. However, great care has to be taken in the design of the RF shielding in order to completely avoid the reception of external interference.

Matching Networks

The above arguments have dealt only with the signal and noise induced in the NMR coil itself. For an NMR experiment power has to be transported to the coil during transmission for NMR excitation. On the other hand, the signal generated inside the coil has to be detected in the preamplifier during reception. For both cases it is common to use cables.

During transmission all of the power should be transferred to the NMR coil and no power should be reflected. This is the so-called power match situation, where the transmitter, the load—in this case the coil—and the cable should have the same **impedance** Z_0. The characteristic impedance Z_0 of the cable does not come from the ohmic resistance, but is given by the inductance L_0 and the capacitance C_0 per unit length of the cable as $Z_0 = (L_0/C_0)^{1/2}$. There are various conventions for the characteristic impedance of coaxial cables. In NMR the most common situation is to use coaxial cables with $Z_0 = 50\ \Omega$. In order to achieve this at the coil, a network is used to match the impedance of the NMR coil to the

impedance of the cable, commonly referred to as the tuning and matching network. This matching network typically consists of capacitors (*12*), potentially in combination with an inductance (*13*).

During reception, the signal has to be transferred to the preamplifier while preserving the SNR of the NMR experiment in the coil. Normally, this is again accomplished using the power match situation where all components have an impedance of 50 Ω. However, some modern preamplifiers have their optimal performance at an input impedance which is not 50 Ω. These preamplifiers can also be useful, in particular in surface coils, to reduce mutual coupling (*4*).

In general the components of the matching network should have low losses. The issues in the design of matching networks strongly depend upon the application and the Larmor frequency or the nucleus observed. While only a few topics in matching network design are addressed in this article, such as electrical balancing, these issues are so many and so varied that they cannot be completely described. For this reason, we refer the reader to the many well-written articles and books concerning matching and tuning networks contained in literature, for example (*14*).

Sensitivity Criteria

The best achievable SNR can be described as intrinsic SNR (*15*). It relates the NMR signal, which originates from the ROI, to the noise originating from the same region of the sample. The ideal SNR, which would be obtained if no additional sources of noise were present, such as ohmic or dielectric losses in the probehead, is the ratio of these two values. This intrinsic SNR, which can be calculated, can be compared to the SNR that is obtained in an experiment in order to get an idea of the performance of a given coil.

As has been indicated with the principle of reciprocity, the sensitivity of a probehead is characterized best by the B_1 field strength that is generated within the sample when a given power P is applied to the probe's input **port**. Therefore, in practice the sensitivity of the probehead at a certain location can be characterized by the $B_1/\sqrt{P}$ ratio. The next section describes several additional tests that can be performed on the workbench as well as in the spectrometer in order to characterize the performance of an NMR probehead.

QUALITY CONTROL AND COIL CHARACTERIZATION

Procedures for quality control are crucial for the comparison of the performance of various NMR coil designs and the evaluation of alterations in sensitivity. Measurements on the workbench are preferred, since they are fast and inexpensive. They allow one to monitor the influence of design changes during the construction of a new probehead, and can also provide a quantitative measurement of the achieved sensitivity (*16*). The ultimate test of an NMR coil, however, is the experiment in the NMR instrument. In this section we outline some basic measurements for the characterization of the properties of an NMR probehead, first on the workbench and then in the NMR instrument.

Workbench Measurements

Most measurements on the workbench detect the frequency dependence of the RF power transmitted through or reflected from the probehead while it is connected to the measurement apparatus through a coupling network. A network analyzer is the most convenient, but also the most expensive, tool for these measurements. In many cases, an RF sweep generator, a reflection bridge, an RF detector, and an *xy*-oscilloscope are sufficient.

One should always bear in mind that the coil characteristics depend on its environment. This means that one should be very careful with the design and layout of the RF laboratory space and the placement of the equipment. For example, the **quality factor** Q of the coil may be diminished by materials with high losses in the vicinity of the coil (even by the workbench itself). In addition, the resonance frequency may change due to inductive coupling to conductive materials (which can happen, in particular, inside the spectrometer).

The key parameters to describe any RF coil are the B_1 field strength and homogeneity, the losses in the probehead, and the losses induced by the sample. In principle, it is possible to directly measure the B_1 field strength and homogeneity on the workbench (e.g. (*17*)), however, since these measurements are difficult to perform, these techniques will not be covered in this article. Instead, we will demonstrate in the next section how these measurements can be performed in the spectrometer. Therefore, the most important parameters of an NMR coil which can

be measured on the bench are the losses in the coil and the losses induced by the sample. These losses are most commonly described by the quality factor. A very common definition of the quality factor Q of a coil is

$$Q = \frac{\omega L}{R} \qquad [3]$$

where L is the inductance and R the total resistance. A high ***Q*** means that the coil has low losses. If the coil interacts with its surroundings —which will happen in an NMR experiment—the Q can be decreased by the additional losses in the environment. In an ideal experimental setup, the losses will only arise from the unavoidable interaction of the magnetic **near field** with the examined parts of the sample. In the probehead, losses in the coil itself and in the coupling network, losses in the electric near field, eddy currents in inductively coupled parts of the probehead, as well as radiative losses, can all contribute to the overall loss and have to be minimized, since these mechanisms lower the SNR.

Three different setups are commonly used to measure the quality factor of the NMR coil:

- The first setup consists of two pickup loops which are mutually decoupled. Bringing the resonator in the vicinity of these loops, one measures the power transferred between the two pickup loops as a function of frequency (*12*). It is important that the pickup loops couple only weakly to the resonator so that they do not dampen its response. Possible measurement configurations are either two loops which partially overlap to minimize direct inductive coupling (*17*) (Fig. 3(a)) or two coaxial loops which are distant enough to avoid significant coupling (Fig. 3(b)). A third possibility, which is only applicable to the characterization of linearly driven coils, is to arrange the pickup loops orthogonally, each loop being at a 45° angle to the B_1 field of the coil (Fig. 3(c)). In all of these setups, the transmit loop couples weakly to the resonator, which in turn is weakly coupled to the receive loop. The power transmitted from the transmit to the receive loop is then proportional to the amplitude of the oscillation in the resonator and therefore represents its frequency response, provided that the coupling between the loops is not frequency dependent over the examined range. The quality factor is obtained from this resonance curve as the ratio of its center frequency and its -3 **dB** bandwidth. In order to check that the coupling between pickup loops and resonator is weak, the same measurement should be done with reduced coupling. There should be no change in the measured Q.
- It is often more convenient to measure the Q of a probehead through its coupling network. With the probehead properly tuned and matched, one determines the frequency response of the reflected power. Dividing the center frequency by the -3 dB bandwidth yields half the quality factor. If instead one would like to directly measure the full quality factor, one can divide the center frequency by the -7 dB bandwidth (*18*). The reference level for these measurements (0 dB attenuation) is a short or an open circuit. One should bear in mind, therefore, that there are many ways that this method of measuring the ***Q*** **factor** can give inaccurate results. For example, discrepancies can arise due to losses in the 50 Ω cable and to variations of the cable's characteristic **impedance** away from 50 Ω, or finally if the coil is not exactly matched to 50 Ω.
- A very sensitive measurement of the quality factor is a combination of the two above. Here, the resonator is accurately matched to 50 Ω and driven from the transmission **port** of the network analyzer. With an additional pickup loop coupled weakly to the resonator, Q can be measured in transmission mode. Q is determined as twice the center frequency divided by the -3 dB bandwidth. The reference level for this measurement is the maxi-

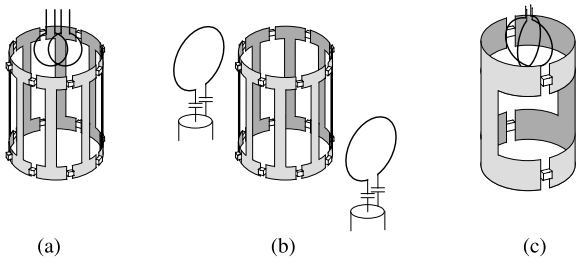

Figure 3 Measurement of the quality factor of an NMR coil with two pickup coils. Direct coupling between the two pickup coils is avoided (a) by partial overlap, (b) by a large distance, or (c) by orthogonality. The last arrangement should only be used when testing a linearly driven coil (i.e., not quadrature).

mum of the resonance curve observed. As above, one should ensure that the presence of the pickup loop does not dampen the resonator.

The relative contributions of the various loss mechanisms can be determined by measuring Q in different loading configurations. Loading the coil with the sample or a phantom of similar conductivity should significantly lower Q, indicating that the losses in the sample dominate. The following simple relation allows one to calculate the sensitivity S of the probehead relative to the sensitivity S_0 of an ideal coil as a function of the quality factors of the empty and loaded coil, Q_{empty} and Q_{loaded}, respectively. This relation holds true provided electric losses in the sample and losses by longitudinal magnetic RF fields can be neglected (*19*):

$$\frac{S}{S_0} = \sqrt{1 - \frac{Q_{\text{loaded}}}{Q_{\text{empty}}}} \qquad [4]$$

A nearly optimal sensitivity can be quite easily achieved for large conducting samples and at high frequencies, but this is much more difficult in microscopy and at low frequencies. There can be several reasons if Q fails to drop upon insertion of a load. Either there are high losses in the coil due to bad conductivity or lossy materials used in the coil construction, or the coil does not generate an RF field in the sample, as could be the case if there are additional resonances in the coupling network. In this case, pickup loops are useful to localize the magnetic RF field.

Efforts to minimize electric and dielectric losses in the sample are of varying importance, depending on the actual application, but it should always be checked whether the Q drops due to these losses. One can get a general idea of the dielectric losses in a typical sample by observing the frequency drop when a sample with a high dielectric constant and very low conductivity (e.g., distilled water) is inserted.

If a coil is double tuned or driven in circular polarization (quadrature), a good isolation between the various **channels** of the coil is another important parameter which can be assessed on the workbench. For clarity, we use the term '**mode**' to describe the intrinsic resonance of the coil itself, while a 'channel' is the port used to connect the individual coil modes to the spectrometer. Quadrature is only possible when the modes are orthogonal and, in addition, the channels are well isolated, meaning little power is transferred between the different channels. This is a requirement for the noise in the two channels to be independent and thus to produce the maximal gain in SNR of up to $\sqrt{2}$ (*20*). If the frequencies of a double tuned probe are not decoupled, additional noise may be received from the second channel. In both cases, strong coupling will make the tuning and matching procedure of the different channels extremely difficult. As a rule of thumb, the power transmitted between the two modes of the probe, as measured between their 50 Ω terminals, should not exceed −20 to −30 dB.

Finally, the efficiency of an RF shield around the coil can be assessed on the workbench. Using a small pickup loop, one can detect RF leakage directly. Another possibility is to slide a solid metal tube over the coil and its shielding. The resonance frequency should not rise and Q should not change, indicating that the coil does not interact with the space outside its shielding.

Measurements in the NMR Instrument

The actual NMR experiment is the final test for a probehead. Besides the SNR of the coil, several properties of a probehead, for instance its performance in the presence of pulsed gradients, can only be tested in the NMR instrument itself. One typically uses different methods to characterize coils that are designed for both transmission and reception, and those coils which are designed for reception only.

Transmit–receive coils can easily be tested by taking advantage of the principle of reciprocity. As outlined in the previous chapter, the SNR obtained in a given experimental setup is proportional to the strength of the RF field B_1 generated by a given power driving the coil that is matched to 50 Ω. Since B_1 depends on the transmit power and the losses, the overall coil performance can be determined by measuring B_1. This is typically accomplished by measuring the duration $t_{90°}$ of a nonselective 90° RF pulse. Given the gyromagnetic ratio γ of the nucleus observed, B_1 can be calculated:

$$B_1 = \frac{1}{\gamma}\frac{2\pi}{4t_{90°}} \qquad [5]$$

To avoid influences from relaxation, it is often preferable to determine the duration of a 360° RF pulse. If the coil has a nonuniform B_1 field, its sensitivity can be determined locally using a phantom which produces a signal only in a well-defined region of the coil. Strictly speaking, B_1 is a good measure of coil performance only if the coil does not pick up noise from extraneous sources. This issue is described in more detail in the following chapter.

Many applications require a good B_1 homogeneity. There are various techniques to measure the B_1 distribution of an NMR coil. A qualitative B_1 map can be acquired from a homogenous phantom using a long prepulse, corresponding to an excitation angle on the order of 3600°, prior to each excitation of a standard imaging sequence (*21*). A single prepulse followed by a fast image acquisition (e.g., FLASH) can equally be used (Fig. 5). Depending on the local B_1, this prepulse corresponds to an excitation angle of an even multiple of 90° in some voxels, leading to bright areas in the acquired image, and to an odd multiple of 90° in others, leading to dark areas. The resolution in B_1 can be increased using larger flip angle prepulses, provided the spatial resolution of the imaging experiment is sufficient to resolve the resulting patterns.

Rotating frame imaging (*22–24*) is a method used to obtain quantitative B_1 maps. A series of images is acquired with increasing pulse duration. For each voxel, the resulting intensity varies as a function of the pulse length and the local B_1 strength. The frequency of this variation divided by the gyromagnetic ratio directly yields the local B_1.

As previously mentioned, these methods are primarily useful in probes designed for both transmission and reception. However, many coils are optimized specifically for reception only, for example the quadrature surface coil for ^{1}H NMR microscopy of the rat heart presented later in this article. In these cases, the methods given above may not be applicable, since the high voltage of the required transmitter pulses may damage or destroy parts of the coil. In these cases, the most important parameters to measure are the SNR and the homogeneity in a typical imaging experiment. These measurements can then be compared to theory, for example, to estimate the performance of the coil.

The methods described in this section present only the most important characterizations that can be performed in the spectrometer. Many applications require additional measurements, such as temperature measurements in human coils, testing of complimentary hardware such as ECG leads, etc., or mechanical stability tests. These considerations should be evaluated on a coil by coil basis.

PREAMPLIFIER AND NOISE MEASUREMENT

The SNR achieved in the receiver coil should be preserved in the receiver chain. The receiver chain consists of several amplification stages, but the overall noise performance is usually determined in the first stage, the preamplifier (*25*). This chapter explains how the SNR is influenced by an amplifier, and how the quality of the NMR instrument can be assessed.

Preamplifier and Noise

The two main properties of an amplifier are its gain and its noise characteristics. The gain is the ratio of the output to the input signal levels. Typical NMR preamplifiers have a gain of about 20 **dB**. To characterize the noise performance, the noise figure F can be used, which is defined as the ratio of the signal-to-noise powers between the input and the output **ports** of the preamplifier (*25*). It is expressed in dB using a reference noise generated by a 50 Ω resistor at a temperature of $T = 290$ K (*26*). The noise figure F is closely related to the equivalent noise temperature T_{eq}, which is the temperature of a $R = 50$ Ω resistor generating the same noise voltage (see Eq. [2]) as the amplifier input:

$$\frac{F}{[\mathrm{dB}]} = 10\log_{10}\left(\frac{\mathrm{SNR}_{\mathrm{In}}^2}{\mathrm{SNR}_{\mathrm{Out}}^2}\right) = 10\log_{10}\left(\frac{290\ \mathrm{K} + T_{\mathrm{eq}}}{290\ \mathrm{K}}\right) \qquad [6]$$

The achievable noise temperatures depend on the transistor type. Bipolar transistors have noise figures down to $F = 1.2$ dB ($T_{eq} = 90$ K), whereas field effect transistors (FET) can achieve noise figures below $F = 0.4$ dB ($T_{eq} = 30$ K). A good spectrometer should have a noise figure below 1 dB, implying that less then 11% of the noise

observed in the recorded signals is generated in the measurement chain.

Noise Measurement

The noise properties of the NMR instrument can be assessed in two steps. First, the noise figure of the whole receiver chain should be measured. Afterwards, one should check whether additional noise sources are picked up by the probehead, for instance due to insufficient shielding. In the following, a relatively simple measurement method is described which can be easily included in a quality assurance protocol without the need for additional instrumentation.

To determine the noise figure of the NMR instrument, a 50 Ω resistor (instead of the receiver coil) is connected to the input of the preamplifier. The "signal" (which of course is only noise) is recorded on the spectrometer, preferably using a somewhat larger than usual acquisition bandwidth, and the standard deviation σ of the noise is computed. Several thousand data points should be acquired in order to get an accurate estimate of the standard deviation. At this point, one should also inspect the signal both in the time domain and after Fourier transformation in the frequency domain in order to identify eventual irregular noise patterns produced by instrumental cross talk or external noise sources. No signal averaging should be performed to ensure that external, incoherent sources of signal do not cancel through destructive interference.

The noise figure of the instrument can be obtained with the hot/cold measurement, as described in the following reference (*26*). In this test, the standard deviation σ of the noise is measured for two temperatures of the 50 Ω resistor, once at actual room temperature ($T_{hot} \approx$ 291–295 K) and once with the resistor submerged in liquid nitrogen ($T_{cold} \approx 77$ K). Care must be taken that the resistance does not change with the change in temperature. One should bear in mind that the use of the ambient temperature is the most convenient way to perform this measurement, however, this method is only an approximation to the standard definition of the noise figure given in Eq. [6].

The noise generated in the resistor at each temperature is known from the theory given in Eq. [2]. Since noise powers add, the noise added by the instrument can be obtained from these two measurements. Its equivalent temperature can be calculated as

$$T_{eq} = \frac{T_{hot} - Y^2 T_{cold}}{Y^2 - 1}, \quad \text{with} \quad Y = \frac{\sigma_{hot}}{\sigma_{cold}} \quad [7]$$

Equation [7] allows one to translate the equivalent temperature into the noise figure F. It should be noted, however, that the noise figure calculated from this equation is only meaningful as long as the probehead is operated at room temperature. If the reception coil is used at a different temperature, for instance if a superconducting probe is used, it is more appropriate to indicate the equivalent noise temperature of the reception chain.

With the procedure described above, the noise characteristics of the complete receiver chain can be assessed. However, as noted earlier, this mostly depends on the performance of the preamplifier.

The measurement of the noise figure and the gain of the preamplifier can be performed much more rapidly on the workbench with commercially available noise-gain analyzers. These use solid state noise generators, whose noise temperature can be changed rapidly by applying different source voltages. In some cases, it can also be interesting to perform the noise measurement with and without the circuitry that protects the preamplifier input during pulse transmission. These networks, which often consist of crossed diodes, can strongly deteriorate the noise performance of the instrument when suboptimal diodes are used in the protection circuit.

Once the noise figure of the instrument has been measured and found to be good, one should verify that no other noise sources are received by the probehead. This can be done by comparing the noise acquired from a 50 Ω resistor at room temperature to the noise acquired from the probehead properly tuned and matched to 50 Ω. Extraneous noise sources lead to a higher noise level in the second measurement, and have to be eliminated by better shielding or other appropriate actions. Finally, one should be aware that high signal levels can also have detrimental effects on the signal-to-noise properties of the preamplifier. For example, high signal levels during testing can saturate the primary transistors of the preamplifier, worsening the response of the preamplifier. In some cases, the protection circuit can also be activated by high signal levels during characterization, resulting in a worse noise figure

than would be obtained during reception of the small NMR signal.

HOMOGENEOUS CYLINDRICAL VOLUME COILS

For many NMR applications the RF field produced by the NMR coil has to be as homogeneous as possible, i.e., for well-defined pulse angles in the NMR experiment or for absolute quantification in NMR spectroscopy. A perfectly homogeneous transverse magnetic field inside a cylinder can be generated by a sinusoidal current distribution

$$\vec{I}_z(\varphi) = I_0 \cdot \sin \varphi \cdot \vec{e}_z \qquad [8]$$

on the surface of the cylinder which is infinite along its cylindrical (z) axis, with φ representing the azimutal angle (*19*, *27*). In practice only approximations of this continuous current distribution are possible by means of discrete conductor elements.

The simplest case is the single rectangular loop which approximates the sine function in two points by two parallel wires with opposite current flow. A better approximation is made in the saddle coil. This type of coil is made from a pair of serial loops with their conductors arranged around a cylinder (see Fig. 14(c)). The saddle coil correctly approximates the sine function at six points, including the zero points of the sine, assuming a 120° opening angle of axial loop elements. In the cosine coil several conducting segments are distributed in parallel with a density N according to $N = N_0 \cos \varphi$ (*28*). The Alderman-Grant resonator consists of two bands of metal on opposite sides of the surface of a cylinder, each subtending a certain azimutal angle which can be optimized for field homogeneity (*29*, *30*). The distributed phase RF coil (*31*) takes advantage of the standing wave on a one wavelength long wound helical conductor. Another promising design for high field homogeneous volume coils is the transmission electron microscopy (TEM) resonator, first proposed by Röschmann (*32*) and further advanced by Vaughan et al. (*33*) and Wen et al. (*34*). A recent development is the so-called litz coil (*35*). Finally there is the birdcage design (*36*), which contains several longitudinal wires arranged symmetrically around a cylinder, which we refer to as rungs, or legs. These legs are connected to form a complete circuit using loops on the ends of the legs, called end-rings. Once a certain length-to-diameter ratio is exceeded for a birdcage, it can theoretically yield any desired transverse homogeneity by varying the number of rungs included in the design. Moreover, quadrature driving and detection is possible, which can lead to a further $\sqrt{2}$ improvement in sensitivity (*20*). Since the birdcage resonator has been the most commonly used homogeneous volume coil in the past we describe it in more detail in the next section.

The Birdcage

The birdcage can be divided into two basic classes: the high-pass birdcage and the low-pass birdcage, with the bandpass birdcage forming a hybrid between the two. All of these types are characterized by the placement of the capacitors. In the high-pass design, for example, the capacitors are located only in the end-ring segments, while the low-pass has the capacitors in the legs. Several papers exist concerning the calculation of the eigenmodes and frequencies in the birdcage (*36–39*). The useful eigenmode for NMR imaging is twofold degenerated and possesses a single standing wave on the end-rings of the birdcage corresponding to the sinusoidal current distribution in the rungs described above.

When designing a birdcage coil, one should decide on the type of birdcage coil to build before starting. The high-pass birdcage has various advantages over the low-pass design, in that there are no capacitors in the legs which produce electrical stray fields in the sample volume. Furthermore no eddy currents induced by switched gradient fields are possible in the end-rings, since the end-ring conductors are separated by capacitors. A high-pass design can also be useful for constructing high frequency birdcages since the higher order inhomogeneous **modes** are at lower frequencies (*37*).

An important feature of the low-pass birdcage is that the frequency of the homogeneous mode is lower than all of the nonusable higher order modes (*36*), and lower than the homogeneous mode of a high-pass birdcage constructed with the same geometry and capacitance. This can be advantageous for the design of coils to be used at low frequencies. Additionally, the low-pass birdcage can be provided with telescopic legs so as to form cylindrical capacitors. This enables tuning via changes in the mechanical length of the coil

without any influence on its symmetry (*40*). However, the fabrication of a telescopic assembly is difficult and a huge variation in length is not possible or desirable with most samples. The parasitic electrical fields of the low-pass birdcage can also be improved by splitting the leg capacitors into two and placing them at the upper and lower end of the legs (*41*).

The so-called bandpass configuration (*42*) uses capacitors in both the end-rings and rungs. The distributed capacitance in this design decreases the effects of propagation near self-resonance as they occur at very high frequencies or very large volumes (*43*). In addition, the design offers the possibility to design birdcages with unusual properties. For example, in (*44*) a modified bandpass birdcage was used simultaneously as a homogeneous transmit coil and as a multi**channel** coil array in reception with increased SNR.

As stated above, the transverse B_1 field homogeneity of the birdcage depends on the number of legs. The more legs there are, the more homogeneous the B_1 distribution will be inside the sample volume, especially in its outer areas (*45*). On the other hand, a lowering of the **quality factor** of a birdcage has been reported with a higher number of legs (*46*) which was considered to be caused by the additional required capacitors. In addition, a suitable compromise has to be found between the desired properties of the coil on the one hand and the work effort and the number of components needed to build the coil on the other.

The length and diameter of the birdcage determine its sensitive volume and should be adapted to the sample volume to be investigated. A maximum sensitivity of the coil is achieved in the middle plane if length and diameter have a ratio of 0.7 (*47*). But in such a situation, the maximum of sensitivity is only valid in the middle plane and often comes at the expense of field homogeneity in axial direction. If the volume of interest is more extended in the z direction, the birdcage must have a longer length to gather the signal from the outlying areas, at the expense of less sensitivity.

Practical Design Considerations

The conductors used to make the birdcage should have low resistance and low inductance (*19*). In terms of microscopy, the coil can often be constructed in an easy and exact manner using flexible material for printed circuit boards, e.g., copper coated PTFE. If this material is double-sided, one has the chance to build foil capacitors directly into the printed design using the plastic substrate as a dielectric (*37*). Certainly the **loss angle tan δ** of the dielectric has to be small, otherwise the quality factor of the coil is severely affected. In our lab, we prefer Arlon AR 450 (Arlon Microwave Materials Division, Bear, Delaware, USA) which contains 70 μm copper foil double-sided on 137 μm PTFE with a capacitance of 29.1 pF/cm^2 and a loss angle of $\tan \delta = 0.0026$ at 1 GHz. As conventional discrete capacitors for microscopy coils, we recommend nonmagnetic ceramic chip capacitors manufactured by ATC (American Technical Ceramics, Huntington Station, NY, USA). These capacitors have high ***Q*** and a sufficiently high breakdown voltage. For birdcage construction, the capacitance tolerance should be small, since deviations in a single capacitor can disturb the symmetry of the birdcage and lead to B_1 inhomogeneity (*48*).

Shielding of the coil is important to diminish the interactions with the surrounding environment. This is especially important for birdcages with dimensions very close to the dimensions of the bore of the magnet or the gradient tube. Interactions with either of these can disturb the normally high field homogeneity of the birdcage if no shield is present. Therefore a good RF shield should eliminate any influence from outside the coil and deliver a well defined boundary for the birdcage so that the functionality of the probehead becomes independent of its operating environment.

A cylindrical shield, in general, increases the resonance frequency of the birdcage and decreases the B_1 field strength in the sample volume. This is more important as the ratio of shield diameter to coil diameter is decreased (*49*). This frequency dependence can be used to build a tuning mechanism (*50*).

In order to avoid eddy currents caused by the switched gradients, the shield should be built from overlapping strips (*51*) so that no **DC** current path is possible around the probe, while the RF currents are still carried by the capacitors made up of the two overlapped strips and the dielectric in-between. The shield conductor itself should be at least several **skin depths** thick, while the loss angle of the dielectric should be as small as possible. It is often advantageous to connect the shield to the RF ground potential at the

connection of the outer conductor of the cable and the coil. However, great care should be taken to ensure that this connection is made with the shortest wire possible, and as a rule of thumb, this wire should be much shorter than 1/10 of a wavelength. For further information regarding proper grounding and shielding principles, please refer to (*12*, *14*, *25*).

A coupling device is necessary to transform the birdcage's **impedance** to that of the transmission line for an optimum signal transfer in the case of both transmission and signal detection. Inductive coupling (*13*) requires a very precise mechanical setup and sometimes can cause problems due to the restricted space in the probehead. However, several different ways exist to couple capacitively into the coil (*37*, *46*, *52–54*). The coupling network itself should disturb the symmetry within the birdcage as little as possible. A symmetric network which uses balancing units is recommended (*12*).

A Probehead for ^{1}H NMR at 11.75 T

An eight rung high-pass birdcage was built for ^{1}H imaging and spectroscopy of perfused rat hearts on a Bruker 11.75 T vertical bore spectrometer. It was etched from 105 μm copper foil on a 50 μm polyester substrate (GTS Flexible Materials LTD, Berkshire, UK). The etching process used ferric chloride, which has to be removed completely after etching any coil to maintain the B_0 homogeneity inside the magnet. The coil has an inner diameter of 21 mm and an overall length of 36 mm to achieve good B_1 homogeneity within a FOV of about 20 mm in z direction. The resonance frequency of 500 MHz was obtained with 10 pF capacitors. Coupling was performed using the balanced network shown in Fig. 4.

The unloaded Q of the coil is 160 and drops to 40 when loaded with a physiological saline solution (cylindrical phantom with 18 mm inner diameter and 40 mm length) which shows that sample noise is the dominant loss mechanism in this coil. The B_1 strength in the center of the coil was 113 μT at a transmitter power of 50 W and showed the desired quadrature gain over that in linear operation. These values correspond to a $B_1/P^{1/2}$ ratio of 16.0 $\mu T/W^{1/2}$. Figure 5 illustrates the field homogeneity in a longitudinal plane on the homogeneous sample. Figure 6 shows a transverse slice of a Langendorff perfused rat heart as an example for application.

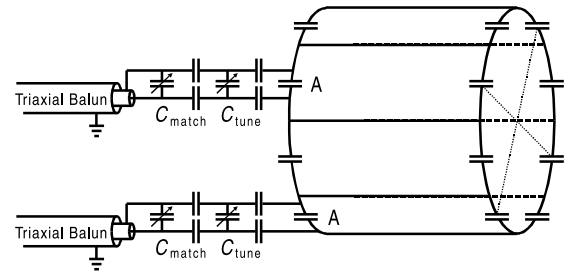

Figure 4 Fully symmetrical capacitive coupling network of the two quadrature channels of the birdcage as described in (*12*) with triaxial baluns for balancing the electrical potentials. The distances between the circuitry elements and the resonator should be kept as short as possible. Capacitors A can be altered to compensate the de-tuning effect when connecting the coupling network. The value of capacitor B can be changed slightly for orthogonalization of the quadrature modes in the birdcage. The capacitors between C_{tune} and the coil are used to adjust the tuning range.

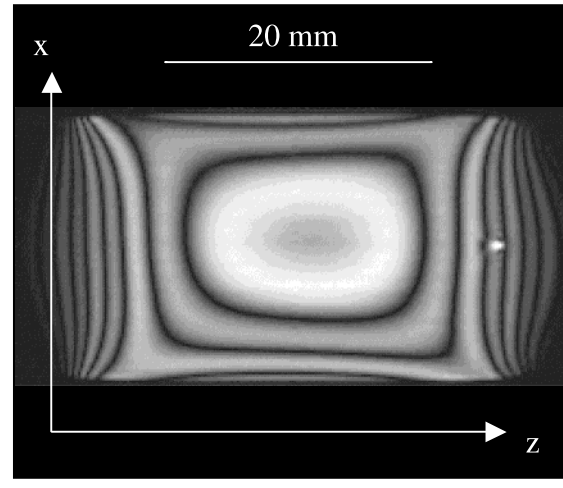

Figure 5 B_1 map. ^{1}H FLASH image after prepulse of 1800° at 11.75 T. Different bright areas correspond to a 10% difference in field strength.

SURFACE COILS

For many applications it is less important to get signal from the whole sample (or patient) than to get as much signal as possible from a small region of interest. In this case, it is advantageous to use a local coil which is adapted in size and shape to the desired field of view. The most important type of such coils is the surface coil (*3*). A surface coil receives a larger signal amplitude from the region of interest than a whole body coil due to the smaller coil diameter and the small distance between coil and the region of interest. Addition-

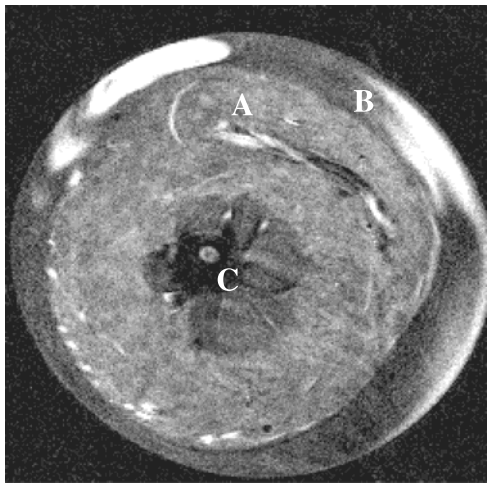

Figure 6 Transverse ^{1}H image of a Langendorff perfused rat heart within a 20 mm diameter NMR glass tube at 11.75 T. In-plane resolution 70 μm, slice thickness 0.2 mm. A: myocardium, B: perfusate, C: left ventricle.

ally, the coil is only loaded by a restricted subvolume of the sample, hence the signal-to-noise is not only improved by higher signal but also by reduced noise. A review article covering local coils is given in (*55*).

Principle Remarks on Surface Coil Design

The first step when designing surface coils is to adapt the coil geometry to the desired region of interest. Generally this means finding a compromise between sensitivity and sensitive volume, since smaller coils produce a higher SNR, but larger coils cover a larger volume. A simple calculation using the Biot-Savart law on the coil axis shows that for a circular coil the penetration depth is about one coil radius, i.e., at this distance a receive coil has about 35% of the sensitivity at its center. When sample losses are negligible, the sensitivity for a fixed voxel size in the coil plane scales with r^{-1}, where r is the radius of the coil. Detailed calculations of optimal coil diameter for a certain penetration depth and theoretical and maximum attainable SNR (*15*, *56*, *57*) give, in principle, similar results. In case of dominating sample losses, the sensitivity is reduced with increasing effective sample volume, i.e., the part of the sample volume the coil "sees." In these cases, the sensitivity scales roughly with r^{-3}, but depends additionally on sample size and geometry (*58*). For best results, it is useful to not only model a coil on the desired region in a heuristic way, but to calculate the B_1 distribution of a given coil geometry (*59*, *60*) and optimize the geometry interactively for an optimal B_1 field distribution for the desired FOV.

The primary disadvantage of a surface coil is its inhomogeneous B_1 field distribution. The B_1 field decreases strongly with the distance from the coil in all directions. This is particularly true in the z direction, where the usable field of view is limited to the coil dimensions, since the B_1 field is directed in the z direction near the coil and thus has no effect on the spin system.

This inhomogeneity has two consequences when the surface coil is used for both transmission and reception. Just as the flip angle is proportional to the B_1 field in transmission mode, the received signal amplitude in receive mode is proportional to B_1 due to the principle of reciprocity. The signal amplitude in this case, therefore, is proportional to $\sin(B_1) \cdot B_1$. In particular, the flip angle variation is not tolerable for, e.g., quantitative relaxation experiments. Even simple imaging methods such as gradient echo imaging suffer from strong shading artefacts due to the transmit inhomogeneity of the surface coil.

Therefore surface coils are often used as receive-only coils, taking advantage of the fact that a body coil is generally available for homogeneous excitation, so that all sequences can be applied. This receive-only mode is preferable in many cases, since the sensitivity characteristic of the receive coil will only affect the local SNR over the FOV.

However, it is necessary to avoid the mutual coupling of transmit and receive coils. Without decoupling, two coils tuned to the same frequency couple strongly when placed near each other, which effectively splits the resonances of the coils, leading to both mismatch and signal loss. Additionally, there is a significant risk of local burns in patient studies if the RF power is adjusted for the volume coil. Finally, the noise of the whole volume can be coupled into the surface coil in receive mode, severely degrading the SNR advantage of the receive-only coil arrangement. This problem is typically solved by detuning the coil not in use either passively by diode switches or actively by **PIN diode** switches (*12*, *61–63*). When implemented properly, this method can reduce the coupling between transmit and receive coils in the range of 20 to 50 **dB**s.

The SNR of a surface coil can be improved by a factor of up to $\sqrt{2}$ by combining two coils into a

quadrature surface coil (*64*). This combination of two coils produces perpendicular B_1 fields of equal amplitude in a restricted region. Common configurations (*65*) are an overlapping coil pair (Fig. 7(a)), and a butterfly/circular coil configuration (Fig. 7(b)), i.e., a combination of an antisymmetric two-loop coil (butterfly) and a circular coil. In any case, the mutual coupling of the coils must be minimized by adjusting current induced by one coil in the other to zero. This is primarily done by adjusting the overlapping region of the two coils, as well as preserving a good symmetry between the two coils. It is important to mention that coupling between two coils of a quadrature surface coil set is generally less critical than for volume coils, since the loaded ***Q* factor** is low (< 50) due to the typically heavy loading seen in surface coils and thus mutual coupling is small.

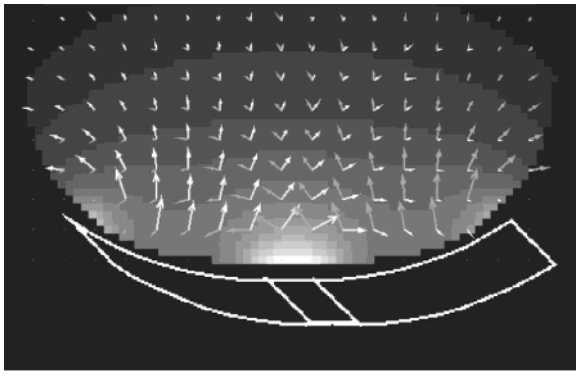

(a)

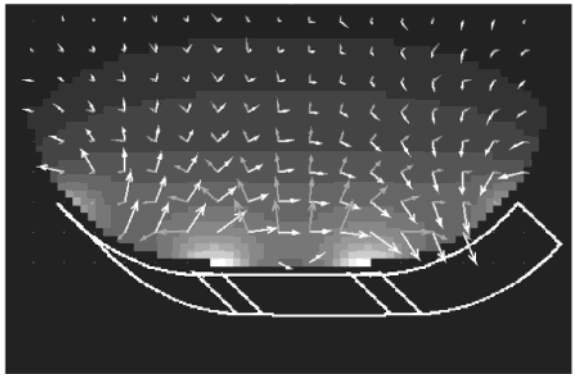

(b)

Figure 7 Two different types of quadrature detection with surface coils: (a) two planar loops and (b) butterfly coil and single loop coil. The brightness of the image is proportional to the computed B_1 amplitude in the *xy* plane. The arrows indicate the direction of the B_1 field of the two different coils. In both cases there is a region in the middle where the arrows of the two coils are perpendicular to each other and of similar magnitude.

However, the gain in SNR of $\sqrt{2}$ can be achieved only if there is no noise correlation between the two coils. Noise correlation is especially present in regions where both coils receive signal, but the quadrature condition is not fulfilled, meaning that the B_1 fields are not orthogonal and of same amplitude. In most cases, the gain in SNR is generally less than $\sqrt{2}$, depending on sample size and geometry and, of course, on coil geometry. When estimating the actual gain in SNR due to quadrature operation, one should also be aware that the quadrature region is, in general, not identical to the region of optimal sensitivity of the single coils. For example, this is certainly not the case for the two coils of a flat overlapping quadrature coil pair (Fig. 7a), or for a flat combination of butterfly and circular coils. However, the sensitive regions do nearly match for a coil pair with a tilt angle of 90°, and similarly for a butterfly/circular coil combination which is placed on half circle around the sample, as described below.

The concept of a set of noninteracting surface coils can be extended to a 'NMR phased array' (*66*). A phased array consists of a set of independent surface coils, each having its own preamplifier, receiver, and analog-to-digital converter (ADC). The separate image data sets from the different coils are combined in a final reconstruction process by suitable combination algorithm. In this way the high SNR of a small surface coil can be achieved in the large FOV of the whole coil set.

As with quadrature coils, the mutual coupling between the coils in such an array must be minimized. In an array of more than two coils, decoupling by adjusting the overlap region is only possible for nearest neighbors. Therefore, in most cases it is necessary to apply an additional decoupling method using the **impedance** of the preamplifier (*4*). The inductive coupling between the coils has its origin in the RF current in the coils, so that one way to minimize the coupling is to reduce the RF current in each coil. This can be achieved without loss in SNR by using preamplifiers with a high reflection coefficient at the input. A suitable coupling network between coil and preamplifier transforms the input impedance of the preamplifier to a high impedance in the coil current path and thus reduces the RF current in

the coil. If the network does not introduce any considerable ohmic losses, this technique does not reduce the SNR. Additionally, GaAs-FETS are available which have their minimum noise figure at high reflection coefficients, so that the SNR can be even better than with 50 Ω matching.

This concept has been implemented on most of clinical NMR scanners in spite of its substantial hardware and software requirements due to the considerable benefits in SNR for most applications. For example, Porter et al. constructed a 16-**channel** receive-only array system for imaging of the brain (*67*). This array showed an increase of SNR of nearly a factor of 3 near the surface while maintaining an SNR comparable to that of a quadrature head coil in the center of the brain. A new development in phased array coils is their use in accelerating image acquisition. Methods such as SMASH and SENSE have been used to achieve several fold decreases in imaging time for 4 to 8 element arrays.

A Quadrature Surface Coil for ^{1}H NMR Microscopy of the Rat Heart at 7 T

As an example, we describe a quadrature receive-only coil for rat heart imaging at 300 MHz using the butterfly/circular coil concept. The schematic of the design is shown in Fig. 8(a), while Fig. 8(b) shows the etching mask of the coil. The B_1 field distribution for this coil is similar to Fig. 7(b) where the basic arrangement can be seen. The loop radius is about 2 cm, which means that the rat heart is completely within the penetration depth of the coil. The circuit board was etched out of a copper plated PTFE foil, which ensures mechanical flexibility and low dielectric losses. As

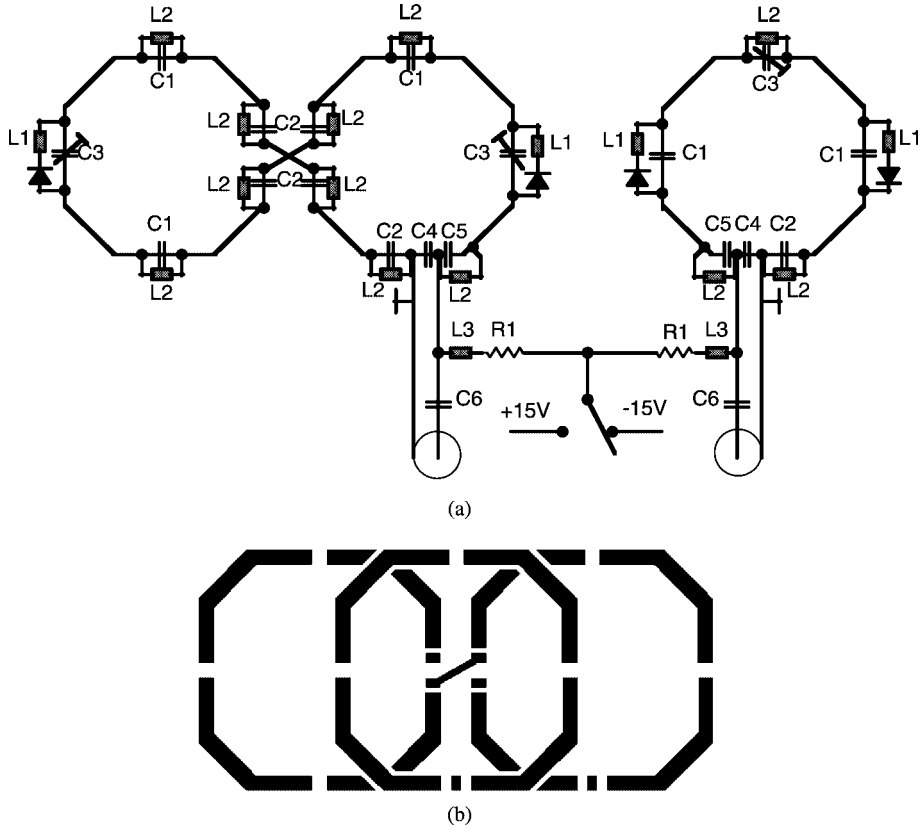

Figure 8 Design of the quadrature surface coil for rat heart imaging. (a) Principle schematics of the butterfly and the single loop coil. The capacitance values and types of the capacitors are: C1 = 12 pF ceramic chip, C2 = 24 pF ceramic chip, C3 = 8 pF ceramic chip parallel with a sapphire trim capacitor 2–8 pF, C4 = 24 pF ceramic chip, C5 = short, C6 = 500 pF. The inductor values are: L1 = 22 nH, L2 > 200 nH, L3 > 500 nH. R1 = 300 Ω. The PIN diodes are UM9401 (Microsemi Corp., Watertown, MA, USA) and have a capacitance of 1.1 pF. The network R1, L3, C6 is for decoupling the DC current path for the PIN diode switches from the RF lines. (b) Etching mask of the quadrature coil.

mentioned earlier, the flexible coil can be placed in a half circle arrangement around the chest of the rat to obtain maximum sensitivity in the heart region. The mutual coupling of the two coils is theoretically zero due to the symmetry of the arrangement.

In order to reduce the electric fields in the sample, the capacitors are distributed at four positions in each loop (*12*). More capacitors are not recommended, as the maximum of the real part of the impedance at one of n capacitors with capacitance $n \cdot C$ is given by $\mathrm{Re}(Z) = L/(n^2RC)$. If n is too large $\mathrm{Re}(Z)$ becomes smaller than 50 Ω and the coupling network would be more complicated than the one described below and cannot be made with capacitors alone.

The coils are pretuned by proper choice of the capacitors for a typical load. Most of the capacitors are ceramic chip capacitors. For fine tuning, sapphire trim capacitors are used, one in the center loop opposite to the cable connection point, and two in the butterfly coil at the outer ends of the coil. In this way the disturbance of the symmetry by tuning is minimized. Each loop has an inductance of about 95 nH, so the total capacitance per loop for 300 MHz is about 3 pF. The capacitors therefore have values of 12 pF or 24 pF, where they are split into two (Fig. 8(a)).

In order to connect the asymmetric coaxial cable to the coil arrangement, the capacitor at the cable connection point was split into two of double capacitance (24 pF), providing a virtual ground point between them. The center conductor of the coaxial cable is connected at one end of these capacitors, with the shield at the virtual ground point. Under a typical load, the Q factor was about 25, so with $R = \omega L/Q \approx 8\ \Omega$, $L \approx 95$ nH, $C \approx 3$ pF, and $n = 8$ the coil was matched to 50 Ω without an additional network. For weaker loading, the capacitor at the cable connection must be split into two to reduce the maximum of the real part of the impedance to 50 Ω as shown in the principle schematics in Fig. 8(a). At the frequency where the real part has its maximum the imaginary part is close to zero.

The signals of the two parts of a quadrature coil have a phase difference of 90°. Therefore they must be combined with a 90° power combiner or a hybrid. A convenient solution is a $\lambda/8$ hybrid which can be built from two pieces of cable and two capacitors (*12*). However, due to its small bandwidth, it is necessary to adjust the capacitance of the two capacitors and the $\lambda/8$ cable length carefully. This can be done with a rather simple setup: a frequency synthesizer tuned to the desired RF frequency (in our example 300 MHz) connected to one **port** on one end of the hybrid, the other port at this end terminated by 50 Ohms, and a two-channel oscilloscope (50 Ohm input impedance) connected to the two ports at the other end. The two capacitors and the $\lambda/8$ cable length are optimized until both oscilloscope channels show equal amplitudes and a phase difference of 90°.

The surface coil is switched off during RF irradiation by the surrounding transmitter coil by PIN diode switches. With bias current 'on,' a PIN diode switch for a receive-only coil forms a high impedance blocking circuit in the RF current path of the coil. This circuit is formed by one of the ceramic chip capacitors of the coil, the PIN diode, and an inductor. The circuit is typically tuned to the operating frequency of the coil by varying the inductance in parallel with the capacitor. With bias current 'off,' the PIN diode switch should not have any influence on the coil. Therefore the PIN diodes must have a capacitance which is small compared to that of the coil capacitor (12 pF). In order to reduce the noise generated by the diode, it is biased by a negative voltage of 15 V when 'off.'

To avoid hot spots, i.e., points with large RF field at the sample surface due to the PIN diode circuits, these circuits are orientated perpendicular to the surface and are kept as small as possible (**SMD** inductor, ceramic chip capacitor).

In order to achieve efficient decoupling (> 20 dB) each part of the coil has two switches. For simplicity, the RF coils themselves are also used as **DC** current paths for the PIN diodes. Therefore all capacitors which interrupt the DC current path are bypassed by nonmagnetic SMD inductors (RF-chokes). This concept has a disadvantage in that the DC current produces a DC magnetic field during RF transmission. Therefore the DC current must be adjusted to be high enough for decoupling, but small enough to keep the B_0 deviation in the range of the inherent inhomogeneities. For this coil we found that a reasonable current is in the range of 50 mA which gives a maximum magnetic flux density of about $1.5 \cdot 10^{-6}$ T corresponding to a Larmor frequency shift of 67 Hz.

The coil has been used for research measurements such as snapshot-FLASH-T_1-imaging for regional blood volume (*68*) and perfusion studies (*69*) in the myocardium of rat hearts *in vivo*. A

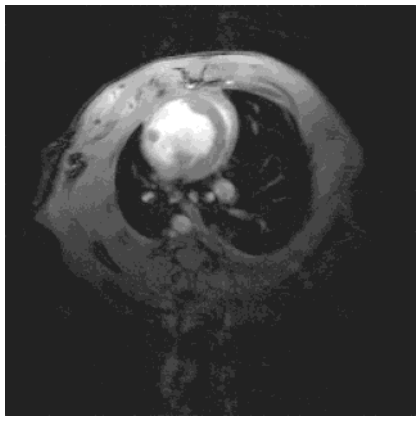

Figure 9 Transverse slice of a ^{1}H cine-FLASH image of a rat with myocardium infarct at 7 T. In-plane resolution 234 μm. Slice thickness 1.5 mm.

typical snapshot-FLASH cross section image of a rat is shown in Fig. 9. The SNR in the heart is about three times as high as with the standard resonator of the system, a linear birdcage resonator with an inner diameter of 7 cm and a length of 12 cm. For RF transmission a home-built probehead with a diameter of 7 cm and a length of 18 cm was used which was also detuned by a PIN diode switch during signal acquisition.

DOUBLE TUNED COILS

NMR measurements on nuclei other than ^{1}H are made difficult by the very low sensitivity of these X nuclei, for example ^{13}C and ^{31}P. This results both from the low natural abundance of these isotopes, which can rarely be enriched in an *in vivo* experiment, and from the Larmor frequency, that is adverse in comparison to ^{1}H. However, even if a very sensitive coil for X nuclei is available or a high SNR can be achieved by averaging, the SNR will still not be sufficient in most cases for positioning or shimming the sample. Therefore, an additional ^{1}H **channel** is desired and is provided in most X-nuclei probeheads. Additionally, this enables the use of SNR-increasing double resonance techniques such as ^{1}H decoupling, nuclear Overhauser enhancement (NOE) or polarization transfer. However, it is not easy to build a double tuned coil that fulfils the two basic requirements: an X channel that shows no decreased sensitivity compared to a single tuned coil, and an ^{1}H channel which allows at least shimming and imaging, and where necessary, double resonance techniques.

Different Principles of Double Resonance

The simplest electric resonant circuit contains an inductor (in our case the NMR coil) and a capacitor. The inductor is the component which usually limits the $\boldsymbol{Q}$ of the circuit. For double resonance a second resonant circuit is needed and therefore at least two inductors and two capacitors. The additional circuit enables resonance at a further frequency but, at the same time, increases the coil losses. These losses are negligible if the total losses are dominated by a different loss mechanism, such as losses in the sample. However, in particular in NMR microscopy and on samples with low resistivity, the SNR can be affected by these additional losses, therefore, much effort has to be spent in order to optimize the sensitivity of the probe.

Double Resonance in the Coupling Network. A very common technique of double tuning a coil is to situate the additional resonance circuit in the coupling network, see, for example (*70–72*). The same NMR receiving coil is used for both frequencies. That means that the probehead has the same B_1 field characteristics for transmit and receive and that these do not have to be determined for both frequencies separately, since the B_1 homogeneity is not affected by the double tuning scheme. However, the coil sensitivity will be diminished by the second circuit when other losses (mostly sample losses) are not dominant (*5*, *12*, *25*, *72*). The reduced efficiency ρ_H of the higher frequency of the NMR coil of a simple double resonant circuit can be expressed as

$$\rho_H \approx \left\{1 + \frac{Q_1 \cdot L_1}{Q_2 \cdot L_2}\right\}^{-(1/2)} \qquad [9]$$

whereas for the lower frequency the reduced efficiency ρ_L is

$$\rho_L \approx \left\{1 + \frac{Q_1 \cdot L_2}{Q_2 \cdot L_1}\right\}^{-(1/2)} \qquad [10]$$

(*25*) L_1 is the inductance of the detection coil and Q_1 its **quality factor**. L_2 and Q_2 are the inductance and the quality factor in the additional resonance circuit (*25*). Equations [9] and [10] are approximations, since the effect of the two matching networks and an eventually needed provision for isolation are neglected. However, the ratio of the two inductances gives an impres-

sion of which of the two frequencies will suffer the majority of loss in sensitivity. In many applications, this will provide a coil which can be used, however, at least at one frequency will experience a significant loss in sensitivity compared to a single tuned coil.

Crossed Coils. The utilization of an additional, lossy resonance circuit does not necessarily mean a decrease of sensitivity. It is also possible to employ the second circuit for signal detection as well. If the circuits are isolated, for example by an orthogonal arrangement of two coils, then there will be no impairment of the performance of either coil by the other. In this crossed coils configuration each coil can be used at its own frequency without loss of sensitivity. Here, different coil designs are imaginable: saddle coils, Helmholtz coils, or single loop coils as well as their combinations. However, a fully independent optimization of the coils can prove difficult because of the geometry of the arrangement. Typically, a compromise has to be made in the performance of one of the coils in such an arrangement. A potential way out of this dilemma is provided by a birdcage in which the two orthogonal channels are used for double tuning (*73*, *74*), although B_1 field inhomogeneities have to be taken into account when considering this type of coil. However, even if two fully equivalent channels were achievable with a good sensitivity and a good B_1 homogeneity, a crossed coils configuration for two different frequencies does not support quadrature drive. This can be understood as a loss of a factor of $\sqrt{2}$ in sensitivity at each frequency compared to an optimized single coil configuration. Still, this design is often used since it offers a relatively uncomplicated approach to a double tuned probe head.

Double Resonance with Two Coupled Receiving Coils. On the opposite end of the spectrum of possible double tuning configurations, one can achieve double tuning by orientating the B_1 fields of the two receiving coils in parallel. In this case, the two circuits directly couple through their respective NMR coils. At the lower frequency currents in the two coils are in phase, at the higher frequency they are of opposite phase (Fig. 10). Since the two coils now are in parallel, an equivalent second coil pair can be orientated orthogonally to the first which can be used to provide quadrature drive and thus improve SNR.

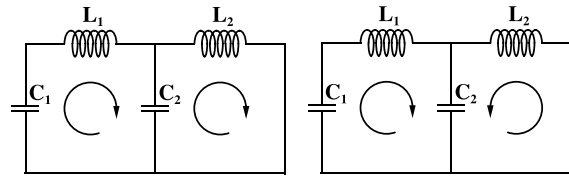

Figure 10 A double resonant circuit needs at least two capacitors and two indecencies. At the lower frequency, the currents will be in phase, while they are of opposite phase at the higher frequency.

There are two fundamentally different configurations of double resonant circuitries which work in this way. In one, the two parallel coils cover the same sample volume while in the other, the sensitive regions of these coils are spatially separated. Hybrids of the two designs are possible and utilized (*75–80*).

In the first case where the coils cover the same sample volume, they will oscillate in phase at the lower frequency and their B_1 fields will interfere constructively. Sensitivity then is optimal. However, at the higher frequency the coils oscillate with opposite phase and the fields interfere destructively in the sample volume. Sensitivity will be diminished more or less according to the ratio of the B_1 field amplitudes. A typical example of this configuration is two concentric birdcages (*78*). The attenuation at the higher frequency may be varied by the coupling between the two birdcages, for example by the ratio of the birdcage diameters or lengths.

The second case of spatially separated coil volumes is very interesting because the sensitivity at both frequencies is not deteriorated since both inductors are used for the detection and the B_1 fields do not interfere destructively. However, realizing this configuration is not easy. In most experiments, the investigation of a continuous sample volume is necessary. However, every coil in this double tuning configuration generates stray fields which can reach into the volumes of the other coils. Due to the opposite phase at the higher frequency, these stray fields lead to destructive interference and hence a loss in sensitivity at the higher frequency. However, in the ideal case of well separated coil volumes, this principle of double tuning is the only one with no additional losses, assuming that the losses are dominated by the Q of the coils. The four ring birdcage (*79*, *80*) we describe in the following is an approximation of this ideal case.

An Example for a Double Tuned Volume Coil: The Four Ring Birdcage

A four ring birdcage can be understood as three single birdcages, where adjacent birdcages share an end-ring. Figure 11 shows a high-pass–high-pass design. The outer birdcages are identical and represent one coil in the double tuning scheme. Resonance of this system means that all three birdcages oscillate in the same fundamental **mode**. However, there are only two resonance frequencies that produce a homogeneous, transversal B_1 field in the center of the coil that can be used for NMR. At these two resonance frequencies, the current distribution in each of the birdcages is sinusoidal, but the inner and outer birdcages are in phase at the lower frequency and of opposite phase at the higher frequency. One of the biggest advantages of this configuration is that the four ring birdcage can be built in such a manner that the birdcages will oscillate at both frequencies with comparable amplitudes, and therefore have similar sensitivities. Thus, the region of sensitivity covers the whole volume of the coil at the lower frequency where the birdcages are in phase. At the higher frequency, however, neighboring birdcages interfere destructively in the plane of the inner rings. Apart from these two zero planes, which represent only a small part of the coil volume, the B_1 field distribution shows adequate sensitivity and homogeneity.

A ^{13}C ^{1}H Four Ring Birdcage for Measurements on Isolated Rat Hearts

The probe described here is used for NMR measurements *in vivo* in a field of 11.75 T at an AMX 500 (Bruker Analytical Instruments, Rheinstetten, Germany). It supports sample tubes of up to 20 mm diameter. The transmit and receive coil is an eight rung four ring birdcage (Fig. 11) made out of 80 μm copper foil and nonmagnetic chip capacitors (ATC, Huntington Station, NY, USA). It is mounted on a glass tube with an outer diameter of 24 mm. Polymers containing carbon compounds as carrier for the copper foil as well as in the whole region of the resonator could not be used due to the resulting disturbance of the ^{13}C signal. Ceramic chip capacitors of 135 pF and 18 pF were used to tune to ^{13}C frequency (125.8 MHz) and ^{1}H frequency (500.2 MHz).

The probehead has an RF shielding with a small distance of only 7.5 mm between the shield and the resonator, due to the small size of the gradient bore. Due to this limitation, the resonator is coupled capacitively (Fig. 4). The ^{13}C

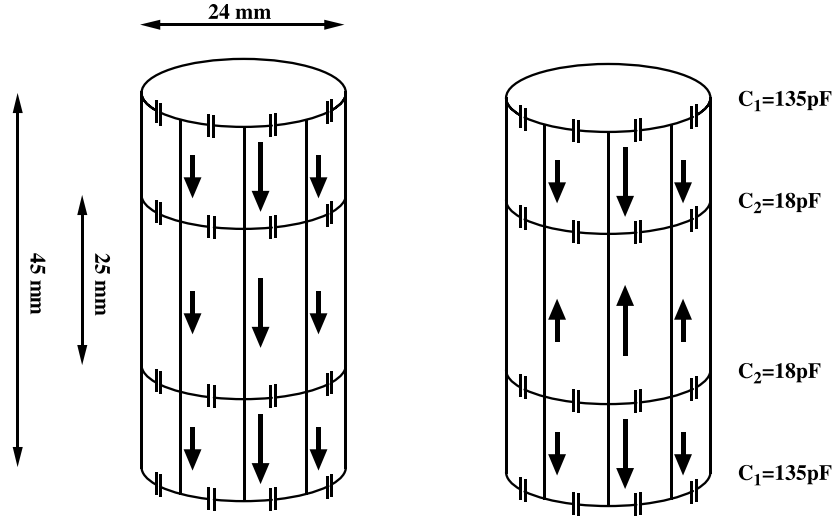

Figure 11 The two modes of the four ring birdcage that generate a homogeneous B_1 field in the center of the coil. At the lower frequency all birdcages oscillate in phase, while at the higher frequency neighboring birdcages have opposite phase. The highpass–highpass four ring birdcage is built from 80 μm copper foil and chip capacitors with values as shown. The coupling network (Fig. 4) couples to an outer ring at the ^{13}C frequency and to an inner ring at the ^{1}H frequency. To decoupage the two frequency channels, additional bandpass filters were employed in the matching network.

frequency is quadrature driven in order to achieve a high sensitivity. A linear driven ^{1}H channel proved sufficient for this application. The ^{13}C channels are driven via an outer ring, and the ^{1}H channel by an inner ring. To improve the isolation between the two frequencies, bandpass filters were integrated into the matching networks, using an inductor in parallel with one of the fixed capacitors in the matching network.

Table 1 shows the measured Q values of the coil. The relatively small Q drop when the coil is loaded by tube with an inner diameter 19 mm, containing physiological saline solution, indicates that sample losses are not the dominant loss in this high resolution coil. Therefore, it is crucial to avoid losses by the second double tuning inductor, as is done in this coil design. A good intrinsic isolation between the two ^{13}C channels (-24 **dB** when unloaded, and -28 dB when loaded) enables quadrature drive at this frequency. No additional isolation adjustments had to be made (*79*). Furthermore, the isolation between ^{1}H and ^{13}C channels is better than -22 dB at both frequencies and thus permits an independent tuning and matching of all three channels. At the spectrometer, the durations of the 90° pulse lengths for ^{13}C and ^{1}H were determined with a phantom (inner diameter 19 mm) containing 110 mM NaCl in D_2O with an additional compartment in the center containing 0.3 ml of 500 mM enriched 1-^{13}C-glucose. For ^{13}C, the 90° pulse length was measured to be 47 μs at a nominal pulse power of 300 W. For the ^{1}H channel, the 90° pulse was 120 μs at a nominal pulse power of 50 W. This corresponds to a B_1 field strength of 497 μT and 49 μT, and a $B_1/P^{1/2}$ ratio of 28.7 $\mu T/W^{1/2}$ and 6.9 $\mu T/W^{1/2}$ for the ^{13}C and ^{1}H channels, respectively. The intensity profile acquired in a homogeneous sample (Fig. 12(a)) shows the B_1 field distribution along the z direction at the ^{13}C frequency. As can be seen, the four ring birdcage is sensitive over its whole volume along the z direction at the lower frequency. In a sagittal ^{1}H FLASH image of a homogeneous water sample, two zero-planes of the ^{1}H frequency at the location of the inner rings can be seen (Fig. 12(b)). They demonstrate the effect of destructive interference of the stray field at the higher frequency.

Table 1 Q Factors of the Double Tuned Birdcage. Loaded with an Inner Diameter 18 mm Tube Containing Physiological Saline Solution the Q Factors Drop by a Factor of 1.4 at the ^{13}C Frequency and by a Factor of 2 at the ^{1}H Frequency

	^{13}C channel A	^{13}C channel B	^{1}H channel
Unloaded	123	139	165
Loaded	88	100	84

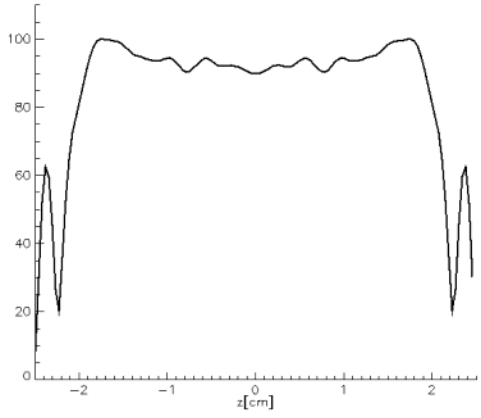

(a)

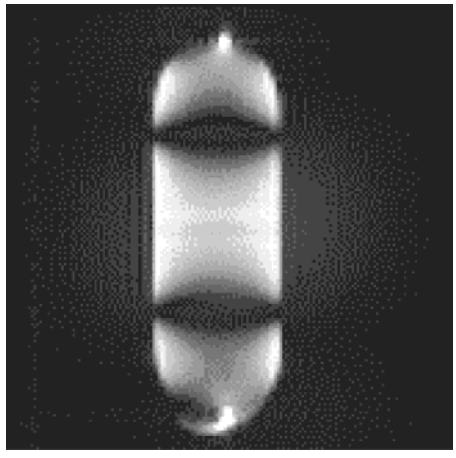

(b)

Figure 12 (a) Intensity profile in z direction in the coil center at the ^{13}C frequency (11.75 T). It was acquired by a ^{13}C CSI sequence on a homogeneous sample of methanol. The coil can be used for detection over its whole length. (b) Sagittal ^{1}H FLASH image of a water phantom at 11.75 T. It demonstrates the ^{1}H sensitivity, while the two zero planes at the location of the inner rings can be seen. In-plane resolution 0.45 mm, slice thickness 0.5 mm.

The probehead was used for spectroscopic investigation of isolated perfused rat hearts (*81*). In this area ^{13}C NMR spectroscopy can provide important information about cardiac metabolism that is not easily accessible by other methods. Perfusing the heart with [2-^{13}C]-acetate will lead to an enrichment of the C4-, C3-, and C2-peaks of glutamate. In Fig. 13(a) two global ^{13}C spectra

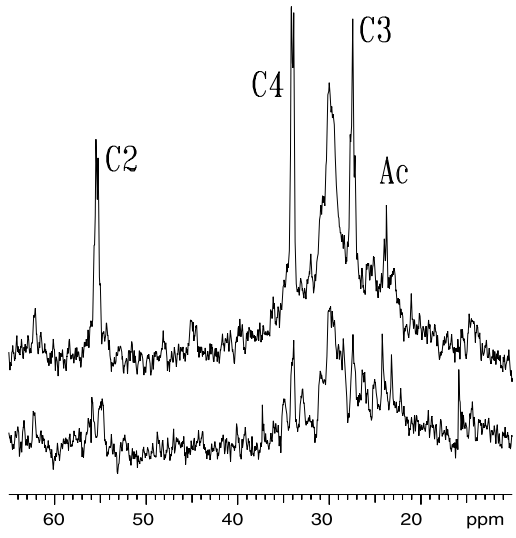

(a)

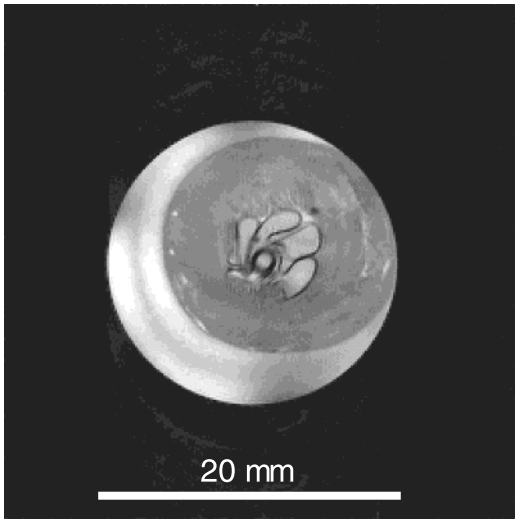

(b)

Figure 13 (a) Global ^{13}C spectra of a perfused rat heart at 11.75 T. Upper spectrum with ^{1}H decoupling and NOE. (b) Transversal ^{1}H FLASH image of the rat heart at 11.75 T. In the left ventricle a pressure balloon can be seen. The right ventricle has collapsed. In-plane resolution 125 μm, slice thickness 1 mm. These measurements are provided courtesy of Claudia Weidensteiner (*81*).

can be seen. The lower is acquired without double resonance techniques in 500 averages with a repetition time of 1.5 s. The upper spectrum has the same acquisition parameters, but is ^{1}H decoupled and nuclear Overhauser enhanced. It is obvious how valuable double resonance techniques are for the quality of the spectra in this application. Besides spectroscopic investigations, NMR imaging can be performed using the coil to aid in areas such as localized spectroscopy and segmentation. As an example, Fig. 13(b) shows a transversal ^{1}H FLASH image obtained with this coil. In this image, a pressure balloon can be seen in the left ventricle, while the right ventricle has collapsed.

MICROSCOPY COILS

NMR microscopy introduces new challenges for the RF coil designer. Since the goal in NMR microscopy is to obtain NMR images with resolution on the order of tens of microns, NMR microscopy necessitates the investigation of small samples at very high frequencies. Whereas in volume coils sample losses are the dominating loss factor, the electric losses in the coil dominate in NMR microscopy. Therefore, a careful design of the coil is of outstanding importance for the sensitivity and thus for the achievable resolution.

Another important point to remember is that in addition to the distortions of B_0 homogeneity which are caused by the sample at these high magnetic fields, additional B_0 distortions will be caused by the RF coil at the small size scales used in NMR microscopy. These distortions are very difficult to correct with shim coils, since most standard shim coils will not be effective over the small dimensions of the sample. Therefore in addition to the normal considerations regarding optimized sensitivity, one must also consider susceptibility issues as well. The principle of reciprocity states that in order to achieve as high a signal as possible from a small sample, the RF coil should be extremely close to the sample. Even though this suggestion is normally correct, the susceptibility discontinuity at the wire surface will cause distortions of the B_0 field at the location of the sample resulting in perturbations of lineshape (*82*) and a loss of sensitivity. This problem can be overcome by various strategies. One possibility is to use a susceptibility matched wire (*25*), which consists of a combination of diamagnetic and paramagnetic materials. Such a susceptibility matched wire may, for example, consist of a core of aluminium ($\chi_m = 2.4 \times 10^{-5}$) coated with copper (magnetic susceptibility $\chi_m = -1 \times 10^{-5}$).

The net susceptibility of the wire can be matched to the susceptibility of air by choosing the right thickness of the copper coating. The use of alloys of two metals with different magnetic susceptibilities leads to wires whose susceptibility

is matched in every partial volume. More expensive materials such as silver, gold, platinum, or titanium can also be used. These show better properties concerning corrosion. A comprehensive discussion about susceptibility matching can be found in (*83*). Another possible approach is to fill the space between coil and sample with a liquid whose magnetic susceptibility is matched to the coil material. This liquid should be an insulator and should not contain the nucleus under investigation. For ^{1}H spectroscopy perflourinated organic liquids have proven to be suitable (*84*).

Since an RF coil has a very low resistance, it needs to be matched to the **impedance** of the coaxial cable by a tuning and matching network. If the coil size is very small, the losses in this network must be taken into account. The properties of the wires in the matching network are also no longer negligible, and care must be taken not to form a loop with dimensions much bigger than the RF coil. If this were to happen, the main part of the B_1 field would be created within the tuning network itself, leading to a very poor filling factor of the RF coil. Therefore, the tuning and matching capacitors should ideally be very close to the RF coil. On the other hand, this may not be desirable because of susceptibility artefacts and interfering electric and magnetic fields.

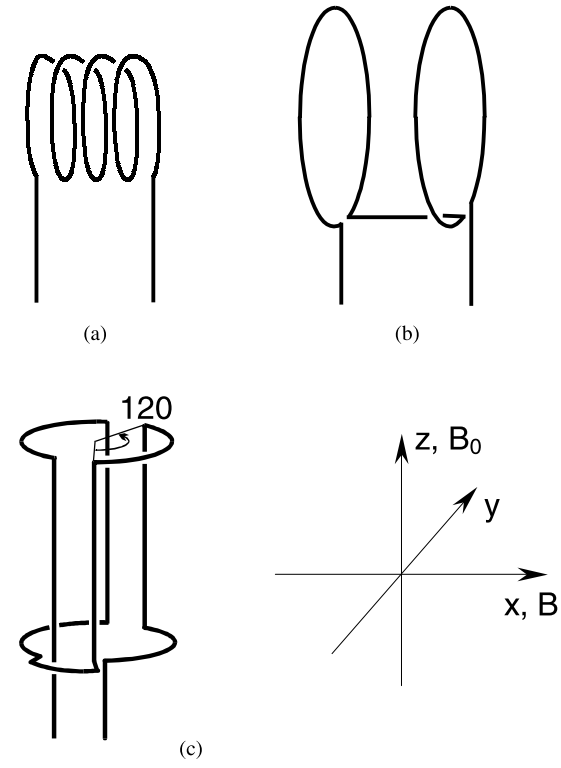

Figure 14 (a) Solenoidal coil, (b) Helmholtz coil, and (c) saddle coil for creation of a B_1 field in x direction. The B_0 field is assumed in z direction.

Coil Types

The most common types of microscopy coils are the solenoidal coil, the Helmholtz coil, and the saddle coil (Fig. 14).

The solenoidal coil (Fig. 14(a)) is the easiest to build. There are only a few construction rules which need to be taken into account to build a coil with optimized geometry for a given volume (*12*). The coil length ought to measure about 80% of the coil diameter. The distance between the turns should be three times the wire radius. The number of turns is limited by the fact that the current will need time to travel down the conductor. If the conductor is too long, there will be phase differences between different parts of the coil which will lead to cancellation of the contributions to the B_1 field from different turns, resulting in a weakening of the field in the coil center. As a rule of thumb, the length of the conductor should not exceed one twentieth of the wavelength (*12*). As a result, the number of turns needs to be reduced with increasing field strength. The solenoidal coil can be built very small in size while retaining a good B_1 homogeneity within the confines of the coil. In cylindrical superconducting magnets, it suffers from the disadvantage that the coil axis must be perpendicular to the B_0 field. This further reduces the usable space, which is already very limited within the magnet bore. Moreover, the sample cannot be accessed without moving the probe out of the magnet.

The Helmholtz coil consists of two parallel loops (Fig. 14(b)) and is almost as simple to build as the solenoidal coil. The best B_1 homogeneity is reached when the gap between these loops is equal to their radius. Thus, for a given sample volume, a Helmholtz coil has twice the diameter of a solenoidal coil, which further reduces the useable space within the magnet bore. However, due to its open structure, a Helmholtz coil is also accessible from the direction perpendicular to the coil axis. This coil is therefore suited for samples with large extensions in one dimension, for example plant stems and roots. However, this open structure is also disadvantageous, as the magnetic energy is less concentrated in the sample, since much of the B_1 field is generated close to the wires. This also holds true for the saddle coil.

The saddle coil (Fig. 14(c)) shows the most complex geometry of these three coil types. The B_1 field is generated primarily by the four vertical wire segments. The best homogeneity is reached for an angular width of 120° (*6*). This configuration is comparable to the leg positions of a six leg birdcage coil, where two legs carry no current (see chapter 'Homogeneous Cylindrical Volume Coils' above). Due to this coil geometry, the B_1 field of a saddle coil is more homogeneous in z direction than that of a Helmholtz coil. The saddle coil can be formed from wire, but it is also often etched from thin copper foil, which is then adhered to glass or PTFE tubing. The latter procedure leads to a high geometric precision, resulting in better B_1 homogeneity. The saddle coil is easily accessible and provides a good 'filling factor' of the usable area in the magnet bore. For these reasons it is widely used in NMR microscopy. However—as mentioned before—these advantages are achieved at the price of decreased sensitivity. Compared to a saddle coil, the sensitivity performance of a solenoidal coil of the same dimensions is approximately three times better (*6*).

Experiments

A 3D imaging experiment at 11.75 T with tumor spheroids (*85*) demonstrates the usefulness of solenoidal coils for NMR microscopy with very small samples. Multicellular spheroids are three dimensional aggregations of cells. In cancer research, spheroids of 400–1000 μm diameter serve as a model to study tumor microregions, since these spheroids have a histological structure closely matching the *in vivo* situation. In this experiment, the process of tumor cell invasion in a co-culture system of tumor spheroids and fetal rat brain aggregates was observed. The solenoidal coil was made from 0.65 mm silver plated copper wire. Three turns with an inner diameter of 2 mm led to a coil length of 2.8 mm. The tune capacitor (chip capacitor 3.7 pF, American Technical Ceramics, Huntington Station, NY) was soldered at a distance of 1.5 cm to the coil. The ***Q* factor** of this coil loaded with physiological buffer solution was measured to be 180. 3D imaging was performed using a T_2 weighted spin-echo sequence with an echo time of 19.4 ms and a repetition time of 1.4 s. A data matrix of $128 \times 64 \times 64$ and two averages led to a total experimental time of 3 h 20 min. An isotropic resolution of 18 μm was achieved. Figure 15 shows a 3D surface reconstruction of the culture. The T_2 weighted imaging technique allows one to distinguish the malignant melanoma spheroid and the fetal rat brain aggregate as well as other morphological areas within the culture.

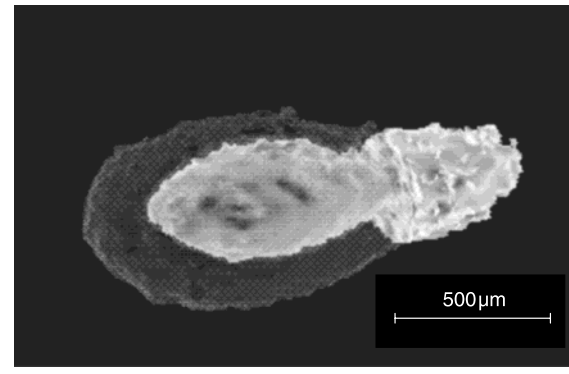

Figure 15 3D surface reconstruction of a culture of malignant melanoma spheroid and fetal rat brain aggregates. For this experiment a solenoidal coil with an inner diameter of 2 mm was used. The T_2 weighted imaging technique allows one to distinguish between the fetal rat brain aggregate (solid) and the malignant melanoma spheroid. Furthermore, within the spheroid the necrobioses (solid) and the viable rim (transparent) can be separated.

The main advantage of saddle coils is demonstrated by an *in vivo* microimaging experiment with *Ricinus communis* seedlings using a 500 MHz vertical bore spectrometer (*86*). Because the stem of the seedling is parallel to the magnet bore, a coil accessible in the z direction must be used for this experiment. In this case, a one turn saddle coil with an inner diameter of 5 mm and a height of 10 mm formed of silver plated copper wire (diameter 0.7 mm) was used. The advantage of the wire construction in this special case is that the vertical opening of the coil (see Fig. 14) can be used to introduce the seedling (diameter 2 mm) into the coil. The Q factor of the empty coil was 300. It dropped to 200 when loaded with a 5 mm tube containing a physiological buffer solution. 2D imaging of a 2 mm slice was performed using a spin-echo sequence (echo time 7 ms, repetition time 1 s, field of view 4 mm). The total acquisition time for a 256×128 image with four averages was 8.5 min. Figure 16 clearly shows the eight bright vascular bundles of the *Ricinus communis* seedling which are connected by the meristematic ring. Although the plant tissue in this part of the stem has a water content of approximately 70%, this area appears dark due to susceptibility artefacts caused by starch grains stored

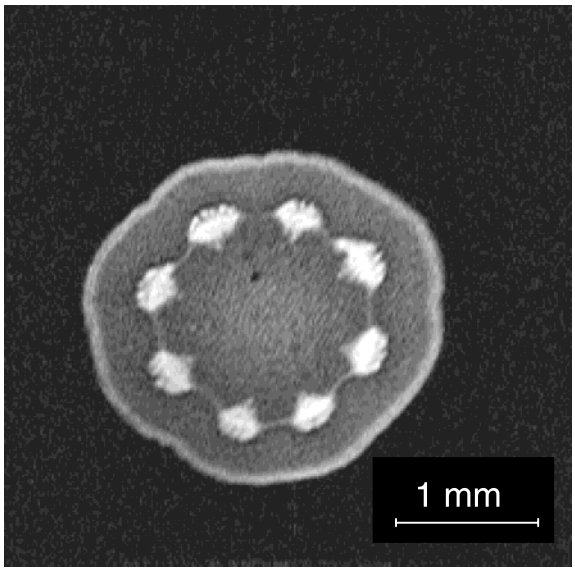

Figure 16 ^{1}H spin echo image of a *Ricinus communis* seedling at 11.75 T. In-plane resolution 15.6 μm, slice thickness 2 mm. The image was acquired using a saddle coil with a diameter of 5 mm. The image shows clearly the eight bright vascular bundles which are connected by the meristematic ring. The stem of the seedling has a diameter of about 2 mm.

in the cells. Only the outer cell layer of the plant, in which no starch is stored, can be seen as a bright ring.

A SMALL GLOSSARY

Channel: A channel is the port used to connect the individual coil modes to the spectrometer.

dB: Decibel. A convenient logarithmic unit for describing quantities within a large range with respect to some reference value. The power P in dB with a reference level P_0 is given by

$$P_{\mathrm{dB}} = -10 \log \frac{P}{P_0}.$$

DC: Direct current. A time invariant current.

Far field: In the far field, an RF coil behaves like an antenna and radiates electromagnetic waves. Thus, energy is flowing away from the source, and the electric and magnetic fields carry the same energy, while they are perpendicular to each other and the direction of propagation. The amplitudes of the fields drop off as $1/(distance)$ in the far field. Formally, the far field can be defined with respect to the distance to the coil by

$$\frac{\lambda}{2\pi} \gg distance$$

where λ is the wavelength.

Impedance: The total opposition to current flow. At **DC** this is given purely by the ohmic resistance. At all higher frequencies there is an additional term given by the reactance of the components. The reactance is a frequency dependent description of storage of power in capacitors and inductors. The total impedance is therefore given by

$$Z = R + X$$

where R is the total ohmic resistance and X is the reactance given by

$$X_L = j\omega L$$

for an inductor L and

$$X_C = \frac{1}{j\omega C}$$

for a capacitor C. The total ohmic resistance R will normally be larger than that observed at **DC** due to the **skin effect**.

Loss angle, tan δ: To describe dielectric losses of a specific material, δ is defined as the angle between the real and the imaginary part of the dielectric constant ε given by

$$\tan \delta = \frac{1}{Q}$$

Mode: When a resonator has more than one resonance frequency each frequency corresponds to a different mode. Each mode has its characteristic current and voltage distribution in the resonator. For example, two quadrature modes of a birdcage coil have the same frequency but different current and field distributions.

Near field: The near field region is the area close to a resonating structure, such as an NMR coil or an antenna. Here the electromagnetic fields are not arranged in a radiative fashion, i.e., the energy contained in the electric field and in the magnetic field at a given point in the near field may not be the same. In addition, the spatial distribution of electromagnetic fields in the near field is highly dependent on the boundary condi-

tions which are determined by the underlying geometry of the resonating structure. Formally, the near field can be defined with respect to the distance to the resonating structure by

$$\frac{\lambda}{2\pi} \ll distance,$$

where λ is the wavelength. The near field is especially important for NMR coils since only magnetic fields in the near field are used for NMR transmission and reception.

PIN diode: PIN diodes are diodes with a broad intrinsic semiconductor region between the p- and n-doped region. They offer the possibility to switch a large RF current by a small **DC** bias current, in contrast to normal PN diodes, where the **DC** current must be at least as large as the amplitude of the RF current.

Port: The point of an electrical connection between two devices. For example, a typical probehead has a port where a cable can be connected.

Q, *Q* factor, or Quality factor *Q*: Components that store energy, such as capacitors and inductors, may be compared in terms of losses by their quality or Q factor. The Q of any such component is the ratio of its ability to store energy to the sum total of all energy losses within the component. In practical terms, this ratio reduces to the formula

$$Q = \frac{X}{R}$$

where X is the reactance of the device given by the imaginary part of its **impedance** and R is the total ohmic resistance.

For a parallel resonant circuit made up of a capacitor and an inductor with the total losses in all the components combined into a resistance R, the Q is given by

$$Q = \frac{\omega L}{R} = \frac{1}{R}\sqrt{\frac{L}{C}}$$

Skin depth: The skin depth describes the thickness of a conductors surface in which the RF currents flow due to the **skin effect**. For typical NMR coils, this is smaller than the geometrical thickness of the wire at all frequencies higher than a few MHz. The skin depth δ is given by

$$\delta = \sqrt{\frac{1}{\pi \nu \sigma \mu_r \mu_0}}$$

where ν is the frequency, σ is the electrical conductivity, μ_r is the relative magnetic permeability of the material, and $\mu_0 = 4\pi \cdot 10^{-7}$.

Skin effect: The tendency of currents at high frequencies to flow only on the outer surface of conductors.

SMD: Surface mount device. A device without leads, designed to be soldered directly on the surface of the circuit board. SMD devices are generally very small and have better RF performance than normal leaded devices. Examples include chip capacitors, inductors, resistors, transistors, and integrated circuits.

REFERENCES

1. Callaghan PT. Principles of nuclear magnetic resonance microscopy, 1. Published edition with corrections. Oxford: Clarendon Press; 1993. 492 pages.
2. Singer JR. Blood flow rates by nuclear magnetic resonance measurements. Science 1959; 130:1652–1653.
3. Ackerman JJH, Grove TH, Wong GG, Gadian DG, Radda GK. Mapping of metabolites in whole animals by ^{31}P NMR using surface coils. Nature 1980; 283:167–170.
4. Roemer PB, Edelstein WA, Hayes CE, Souza SP, Mueller OM. The NMR phased array. Magn Reson Med 1990; 16:192–225.
5. Schnall M. Probes tuned to multiple frequencies for *in-vivo* NMR. In: Diehl P, Fluck E, Günther H, Kosfeld R, Seelig J, editors. *In-vivo* magnetic resonance spectroscopy I. Berlin: Springer; 1992. p 33–63.
6. Hoult DI, Richards RE. The signal-to-noise ratio of the nuclear magnetic resonance experiment. J Magn Reson 1976; 24:71–85.
7. Hill HDW, Richards RE. Limits of measurement in magnetic resonance. J Phys E: Sci Instrum 1968; 1:977–983.
8. Doty FD, Entzminger G, Hauck CD, Staab JP. Practical aspects of birdcage coils. J Magn Reson 1999; 138:144–154.
9. Guéron M, Leroy JL. NMR of water protons. The detection of their nuclear-spin noise, and a simple determination of absolute probe sensitivity based on radiation damping. J Magn Reson 1989; 85: 209–215.
10. Johnson JB. Thermal agitation of electric charge in conductors. Phys Rev 1934; 32:97–109.
11. Hoult DI, Lauterbur PC. The sensitivity of the Zeugmatographic experiment involving human samples. J Magn Reson 1979; 34:425–433.

12. Chen CN, Hoult DI. Biomedical magnetic resonance technology. Bristol: Adam Hilger; 1989. 340 pages.
13. Decorps M, Blondet P, Reutenauer H, Albrand JP, Remy C. An inductively coupled, series-tuned NMR probe. J Magn Reson 1985; 65:100–109.
14. The ARRL handbook for radio amateurs, Danzer P, editor. 77th edition. The American Radio Relay League, 2000, 1200 pages.
15. Edelstein WA, Glover GH, Hardy CJ, Redington RW. The intrinsic signal-to-noise ratio in NMR imaging. Magn Reson Med 1986; 3:604–618.
16. Chen C-N, Sank VJ, Cohen SM, Hoult DI. The field dependence of NMR imaging I. Laboratory assessment of signal-to noise ratio and power deposition. Magn Reson Med 1986; 3:722–729.
17. Darrasse L, Kassab G. Quick measurement of NMR-coil sensitivity with a dual-loop probe. Rev Sci Instrum 1993; 64:1841–1844.
18. Doty FD, Connick TJ, Ni XZ, Clingan MN. Noise in high power, high frequency double tuned probes. J Magn Reson 1988; 77:536–549.
19. Link J. The design of radiofrequency probes with homogeneous radiofrequency fields. In: Diehl P, Fluck E, Günther H, Kosfeld R, Seelig J, editors. *In-vivo* magnetic resonance spectroscopy I. Berlin: Springer; 1992. p 3–31.
20. Chen CN, Hoult DI, Sank VJ. Quadrature detection coils—A further $\sqrt{2}$ improvement in sensitivity. J Magn Reson 1983; 54:324–327.
21. Roffmann WU, Zelaya FO, Crozier S, Doddrell DM. Direct visualization of B_1 inhomogeneity by flipangle dependency. Proceedings of the 4th ISMRM 1996, 1444.
22. Hoult DI. Rotating frame zeugmatography. J Magn Reson 1979; 33:183–197.
23. Talagala SL, Gillen J. Experimental determination of three-dimensional RF magnetic field distribution of NMR coils. J Magn Reson 1991; 94:493–500.
24. Murphy-Boesch J, So GJ, James TL. Precision mapping of the B_1 field using the rotating-frame experiment. J Magn Reson 1987; 73:293–303.
25. Hoult DI. The NMR receiver: A description and analysis of design. Prog NMR Spectros 1978; 12:41–77.
26. Adler R, Espersen GA. Description of the noise performance of amplifiers and receiving systems. Proc IEEE 1963; 51:436–442.
27. Mascart EE, Joubert JF. Leçons sur l'electricité et le magnétisme. Paris: Masson; 1882. 736 pages.
28. Breuer H. Small NMR probe for use in inhomogeneous fields. Rev Sci Instrum 1965; 36:1666–1667.
29. Alderman OW, Grant DM. J Magn Reson 1979; 36:447.
30. Kost GJ, Anderson SE, Matson GB, Conboy CB. A cylindrical-window NMR probe with extended tuning range for studies of the developing heart. J Magn Reson 1989; 82:238–252.
31. Hinshaw WS. Gauss RC. Disributed phase RF coil. Patent, 1984, USA, 4,439,733.
32. Röschmann PKH. High-frequency coil system for a magnetic resonance imaging apparatus. Patent, 5-24-1988, US, 4,746,866.
33. Vaughan JT, Hetherington HP, Otu JO, Pan JW, Pohost GM. High frequency volume coils for clinical NMR imaging and spectroscopy. Magn Reson Med 1994; 32:206–218.
34. Wen H, Chesnick AS, Balaban RS. The design and test of a new volume coil for high field imaging. Magn Reson Med 1994; 32:492–498.
35. Doty FD, Entzminger G, Hauck CD. Error-tolerant RF Litz coils for NMR/MRI. J Magn Reson 1999; 140:17–31.
36. Hayes CE, Edelstein WA, Schenck JF, Mueller OM, Eash M. An efficient, highly homogeneous radiofrequency coil for whole-body NMR imaging at 1.5 T. J Magn Reson 1985; 63:622–628.
37. Watkins JC, Fukushima E. High-pass bird-cage coil for nuclear-magnetic resonance. Rev Sci Instrum 1988; 59:926–929.
38. Tropp J. The theory of the bird-cage resonator. J Magn Reson 1989; 82:51–62.
39. Harpen MD. Equivalent circuit for birdcage resonators. Magn Reson Med 1993; 29:263–268.
40. Holcomb WG, Gore JC. A variable frequency birdcage resonator for imaging at high field. Proceedings of the 5th SMR, 1987, 111–112.
41. Komorski RA, Newton JEO, Cardwell D, Sprigg J, Pearce J, Karson CN. *In vivo* ^{19}F spin relaxation and localized spectroscopy of fluoxetine in human brain. Magn Reson Med 1994; 31:204–211.
42. Edelstein WA, Schenck JF, Mueller OM. Radio frequency field coil for NMR. Patent, 1987, USA, 4,680,548.
43. Harpen MD. Cylindrical coils near self-resonance. Magn Reson Med 1993; 30:489–493.
44. Leussler C, Stimma J, Röschmann P. The bandpass birdcage resonator modified as a coil array for simultaneous MR acquisition. Proceedings of the 5th ISMRM, 1997, 176.
45. Sotgiu A, Hyde JS. High-order coils as transmitters for NMR imaging. Magn Reson Med 1986; 3:55–62.
46. Crozier S, Luescher K, Forbes LK, Doddrell DM. Optimized small-bore, high-pass resonator designs. J Magn Reson B 1995; 109:1–11.
47. Bottomley PA, Charles HC, Roemer PB, Flamig D, Engeseth H, Edelstein WA, Mueller OM. Human *in vivo* phosphate metabolite imaging with ^{31}P NMR. Magn Reson Med 1988; 7:319–336.
48. Jin J, Shen G, Perkins T. On the field inhomogeneity of a birdcage coil. Magn Reson Med 1994; 32:418–422.
49. Collins CM, Li S, Yang QX, Smith MB. A method for accurate calculation of fields produced by the shielded birdcage coil: B_1 strength and homogeneity as a function of shield geometry. Proceedings of the 3rd ISMRM, 1995, 184.

50. Dardzinski BJ, Williams GD, Li S, Collins CM, Smith MB. A birdcage coil with RF shield tuning for application at 9.4 tesla. Proceedings of the 3rd ISMRM, 1995, 993.
51. Krause N. Hochfrequenzfeld-einrichtung in einer kernspinresonanz-apparatur. Patent, 3-3-1983, Germany, DE3133432A1.
52. Sank VJ, Chen CN, Hoult DI. A quadrature coil for the adult human head. J Magn Reson 1986; 69:236–242.
53. Lanz T, von Kienlin M, Behr W, Haase A. A double tuned ^{31}P-^{1}H-four-ring birdcage. Proceedings of the 13th ESMRMB, 1996, 653.
54. Warnking J, Lanz T, Weisser A, Haase A, von Kienlin M. A fully symmetric capacitive coupling scheme for small birdcage resonators. Proceedings of the 15th ESMRMB, 1998, 261.
55. Kneeland JB, Hyde JS. High-resolution MR imaging with local coils. Radiology 1989; 171:1–7.
56. Haase A, Jänicke W, Frahm J. The influence of experimental parameters in surface-coil NMR. J Magn Reson 1984; 56:401–412.
57. Edelstein WA, Foster TH, Schenck JF. The relative sensivity of surface coils to deep lying tissues. Proceedings of the 4th SMR, 1985, 964–965.
58. Suits BH, Garroway AN, Miller JB. Surface and gradiometer coils near a conducting body: The lift-off effect. J Magn Reson 1998; 135:373–379.
59. Keltner JR, Carlson JW, Roos MS, Wong ST, Wong TL, Budinger TF. Electromagnetic fields of surface coil *in vivo* NMR at high frequencies. Magn Reson Med 1991; 22:467–480.
60. Wang J, Reykowski A, Dickas J. Calculation of the signal-to-noise ratio for simple surface coils and arrays of coils. IEEE Trans Biomed Eng 1995; 42:908–917.
61. Beck BL, Duensing GR. Design of decoupling circuits for patient safety. Proceedings of the 5th ISMRM, 1997, 1526.
62. Boskamp EB. Improved surface coil imaging in MR: Decoupling of the excitation and receiver coils. Radiology 1985; 157:449–452.
63. Edelstein WA, Hardy CJ, Mueller OM. Electronic decoupling of surface coils for NMR imaging and spectroscopy. J Magn Reson 1986; 67:156–161.
64. Hyde JS, Jesmanowicz A, Grist TM, Froncisz W, Kneeland JB. Quadrature detection surface coil. Magn Reson Med 1987; 4:179–184.
65. Merkle H, Garwood M, Ugurbil K. Dedicated circularly polarized surface coil assemblies for brain studies at 4 T. Proceedings of the 12th SMR, 1993, 1358.
66. Roemer PB, Edelstein WA. Ultimate sensitivity limits of surface coils. Proceedings of the 6th SMR, 1987, 410.
67. Porter JR, Wright SM, Reykowski A. A 16-element phased-array head coil. Magn Reson Med 1998; 40:272–279.
68. Kahler E, Waller C, Rommel E, Hiller KH, Voll S, Broich A, Hu K, Schnackerz KD, Bauer WR, Ertl G, Haase A. Quantitative regional blood volume studies in rat myocardium *in vivo*. Magn Reson Med 1998; 40:517–525.
69. Belle V, Kahler E, Waller C, Rommel E, Voll S, Hiller KH, Bauer WR, Haase A. In vivo quantitative mapping of cardiac perfusion in rats using a noninvasive MR spin-labeling method. J Magn Reson Imaging 1998; 8:1240–1245.
70. Schnall MD, Subramanian VH, Leigh JS, Gyulai L, Laughin A, Chance B. A technique for simultaneous ^{1}H and ^{31}P NMR at 2.2 T *in vivo*. J Magn Res 1985; 63:401–405.
71. Bolinger L, Prammer M, Leigh JSJ. A multiple-frequency coil with a highly uniform B_1 field. J Magn Res 1989; 81:162–166.
72. Rath AR. Design and performance of a double-tuned birdcage-coil. J Magn Res 1990; 86:488–495.
73. Joseph PM, Lu D. A technique for double resonance operation of birdcage imaging coils. IEEE Trans Med Imag 1989; 8:286–294.
74. Lanz T, Weisser A, Ruff J, Haase A. A double tuned ^{1}H ^{23}Na birdcage resonator for *in vivo* measurements on mice. Proceedings of the 16th ESMRMB, 1999, 139.
75. Grist TM, Kneeland JB, Jesmanowicz A, Froncisz W, Hyde JS. Double resonance ^{31}P, ^{1}H MRS and MRI of human organs using the loop-gap resonator: Techniques and clinical applications. Proceedings of the 5th SMR, 1986, 187–188.
76. Fitzsimmons JR, Brooker HR, Beck B. A transformer-coupled double-resonant probe for NMR imaging and spectroscopy. Magn Reson Med 1987; 5:471–477.
77. Fitzsimmons JR, Brooker HR, Beck B. A transformer-coupled double-resonant probe system for NMR imaging and spectroscopy. Proceedings of the 6th SMR, 1987, 98.
78. Fitzsimmons JR, Beck BL, Brooker HR. Double resonant quadrature birdcage. Magn Reson Med 1993; 30:107–114.
79. Murphy-Boesch J, Srinivasan R, Carvajal L, Brown TR. Two configurations of the four-ring birdcage coil for ^{1}H imaging and ^{1}H-decoupled ^{31}P spectroscopy of the human head. J Magn Reson B 1994; 103:103–114.
80. Lanz T, von Kienlin M, Behr W, Haase A. A double tuned four-ring birdcage for *in vivo* ^{31}P-nuclear magnetic resonance spectroscopy at 11.75T. MAGMA 1997; 5:243–246.
81. Weidensteiner C, Lanz T, Horn M, Neubauer S, Haase A, von Kienlin M. Three-dimensional (13)C-spectroscopic imaging in the isolated infarcted rat heart. J Magn Reson 2000; 143:17–23.
82. Fuks LF, Huang FSC, Carter CM, Edelstein WA, Roemer PB. Susceptibility, lineshape, and shimming in high-resolution NMR. J Magn Reson 1992; 100:229–242.

83. Doty FD, Entzminger G, Yang YA. Magnetism in high-resolution NMR probe design. I: General methods. Concepts Magn Reson 1998; 10:133–156.
84. Olson DL, Peck TL, Webb AG, Magin RL, Sweedler JV. High-resolution microcoil ^{1}H-NMR for mass-limited, nanoliter-volume samples. Science 1995; 270:1967–1970.
85. Brandl M, Tonn J-C, Kotitschke K, Goldbrunner R, Kerkau S, Haase A. Quantitative NMR microscopy of mutlicellular tumor spheroids and confrontation cultures. Magn Reson Med 1995; 34:596–603.
86. Verscht J, Kalusche B, Köhler J, Köckenberger W, Metzler A, Haase A, Komor E. The kinetics of sucrose concentration in the phloem of individual vascular bundles of the ricinus communis seedling measured by nuclear magnetic resonance imaging. Planta 1998; 205:132–139.

(Top row, left to right) **Axel Haase, Florian Odoj, Markus von Kienlin, Jan Warnking, Florian Fidler, Alexander Weisser** (Bottom row) **Mathias Nittka, Eberhard Rommel, Titus Lanz, Bernhard Kalusche, Mark Griswold**

All of the authors have worked on coil development for NMR in the Department of Biophysics at the University of Würzburg. **Axel Haase** is currently the Dean of the Department of Biophysics. **Florian Odoj** did his Ph.D. work at the University of Würzburg on superconducting probeheads and is currently the Technical Manager for the coil company RAPID Biomedical in Würzburg. **Markus von Kienlin** is the Head of the MR Imaging and Spectroscopy at Hoffmann-La Roche Pharmaceuticals. While in Würzburg, he finished his habilitation thesis which focused on localised spectroscopy. **Jan Warnking** did his diploma thesis in Würzburg on optimising coupling networks for double tuned birdcage coils and is currently working on his Ph.D. thesis at the University of Grenoble, France in the area of fMRI. **Florian Fidler** is currently a doctoral student in Würzburg concentrating on cardiac perfusion measurements and has through this work constructed several noise optimised preamplifiers. **Alexander Weisser** is in the process of finishing his Ph.D. which dealt with the optimisation of homogeneous volume coils, and is an engineer at RAPID Biomedical. **Mathias Nittka** has recently finished his Ph.D. in the area of phased array coils, and is currently working at Siemens Medical on sequence design. **Eberhard Rommel** is an instructor at the University of Würzburg and directs several NMR research projects on mice at the Department of Biophysics in Würzburg. **Titus Lanz** is currently working on his Ph.D. thesis on superconducting coils for NMR microscopy and double tuned volume coils for NMR spectroscopy and imaging. **Bernhard Kalusche** worked on high resolution NMR microscopy in plants and is currently a post doctoral researcher at the Klinikum Großhadern at the University of München in the area of neuroradiology. **Mark Griswold** is currently working on his Ph.D. thesis at the University of Würzburg concentrating on phased array coils and their application to partially parallel imaging.